Journal of Environmental Management 360 (2024) 121120

Contents lists available at ScienceDirect

Journal of Environmental Management

journal homepage: www.elsevier.com/locate/jenvman

Research article

Integrating water quality data with a Bayesian network model to improve spatial and temporal phosphorus attribution: Application to the Maumee River Basin

Zihan Wei [a,*,1], Sarfaraz Alam [a,b,1], Miki Verma [c,1], Margaret Hilderbran [b], Yuchen Wu [d], Brandon Anderson [b], Daniel E. Ho [b,2], Jenny Suckale [a,2]

[a] Department of Geophysics, Stanford University, Stanford, 94305, CA, USA
[b] Regulation, Evaluation, and Governance Lab, Stanford University, Stanford, 94305, CA, USA
[c] Symbolic Systems Program, Stanford University, Stanford, 94305, CA, USA
[d] Department of Statistics, Stanford University, Stanford, 94305, CA, USA

ARTICLE INFO

Dataset link: https://doi.org/10.5281/zenodo.8132662, https://doi.org/10.5281/zenodo.8132656

Keywords:
Water quality
Phosphorus source attribution
Network model
Approximate Bayesian Computation
Maumee River Basin
Agriculture

ABSTRACT

Surface water nutrient pollution, the primary cause of eutrophication, remains a major environmental concern in Western Lake Erie despite intergovernmental efforts to regulate nutrient sources. The Maumee River Basin has been the largest nutrient contributor. The two primary nutrient sources are inorganic fertilizer and livestock manure applied to croplands, which are later carried to the streams via runoff and soil erosion. Prior studies of nutrient source attribution have focused on large watersheds or counties at annual time scales. Source attribution at finer spatiotemporal scales, which enables more effective nutrient management, remains a substantial challenge. This study aims to address this challenge by developing a generalizable Bayesian network model for phosphorus source attribution at the subwatershed scale (12-digit Hydrologic Unit Code). Since phosphorus release is uncertain, we combine excess phosphorus derived from manure and fertilizer application and crop uptake data, flow information simulated by the SWAT model, and in-stream water quality measurements using Approximate Bayesian Computation to derive a posterior that attributes phosphorus contributions to subwatersheds. Our results show significant variability in subwatershed-scale phosphorus release that is lost in coarse-scale attribution. Phosphorus contributions attributed to the subwatersheds are on average lower than the excess phosphorus estimated by the nutrient balance approach currently adopted by environmental agencies. Fertilizer contributes more soluble reactive phosphorus than manure, while manure contributes most of the unreactive phosphorus. While developed for the specific context of Maumee River Basin, our lightweight and generalizable model framework could be adapted to other regions and pollutants and could help inform targeted environmental regulation and enforcement.

1. Introduction

Despite decades of expenditures and efforts devoted to cleanup and mitigation, surface water pollution remains a major environmental concern (Howarth et al., 2000; Keiser and Shapiro, 2019; Downing et al., 2021). While pollution in urban areas has decreased alongside upgrades to wastewater treatment systems (Stets et al., 2020), water quality has been slow to improve in agricultural areas (Stoddard et al., 2016; Stets et al., 2020). Although some regions have seen reduced agricultural pollution following advancements in nutrient management and tillage practices (Stammler et al., 2017), many others have shown no significant improvement (Oliver et al., 2017; Stets et al., 2020; Carleton and Washington, 2021) or even continued degradation (Stoddard et al., 2016).

Unlike the point sources in urban areas such as wastewater treatment plants and factories, pollution in agricultural areas comes primarily from unregulated, nonpoint sources, namely, the runoff from extensive agricultural lands (Baker, 1992; Parry, 1998; Carpenter et al.,

* Corresponding author.
E-mail addresses: zihanwei@stanford.edu (Z. Wei), szalam@stanford.edu (S. Alam), meverma@stanford.edu (M. Verma), mhilderbran@law.stanford.edu (M. Hilderbran), wuyc14@stanford.edu (Y. Wu), banderson@law.stanford.edu (B. Anderson), dho@law.stanford.edu (D.E. Ho), jsuckale@stanford.edu (J. Suckale).

[1] Joint First Authors.
[2] Equal co-supervision.

https://doi.org/10.1016/j.jenvman.2024.121120
Received 24 September 2023; Received in revised form 22 April 2024; Accepted 7 May 2024

1998; Ongley et al., 2010; Shen et al., 2012). The pollutants loaded in runoff are nutrients that include various forms of phosphorus and nitrogen from inorganic fertilizer and manure produced by livestock raised in concentrated animal feeding operations (CAFOs) (Baker, 1992; Kumar et al., 2013). Excessive application of manure and inorganic fertilizer can result in higher than optimal nutrient levels in shallow soil layers, which causes nutrient loss in runoff from agricultural land to surge (Higgs et al., 2000; Weil and Brady, 2017) and results in eutrophication (EWG, 2022). The nutrient loss is worsened by modifications to the landscape brought by large-scale agriculture, such as the loss of buffer zones like riparian vegetation and wetlands that mitigate agricultural runoff (e.g., Gilliam, 1994; Jordan et al., 2003; Zedler, 2003; Chase et al., 2016).

These challenges highlight that agricultural areas require different interventions than urban areas. For example, targeted management could optimize agricultural nutrient input to ensure stable crop yield while reducing pollution but necessitates attributing pollution to specific sources. Detailed attribution of agricultural pollution to specific locations, time, and source types remains a highly underdetermined problem because of the diverse and copious pollution sources over extensive landscapes and the lack of water-quality data with high spatiotemporal resolution (OC Interagency WQI Workgroup, 2017). Information about CAFO manure production and inorganic fertilizer application can help constrain the possible pollutant inputs (Falcone, 2021) at different locations (ELPC, 2014) but it does not specify the loss of pollutants into waterways. The USGS water-quality stations provide direct measurements of nutrient loads at daily time scales but are spatially sparse (USGS, 2016; NCWQR, 2022). Neither of these data sets is sufficient in isolation to attribute pollution to specific sources, but integrated into a joint data-model framework they inform a probabilistic connection between sources and pollutant.

The goal of this paper is to advance our ability to attribute phosphorus release to different sources at the subwatershed scale by integrating water-quality observations, phosphorus input information, and hydrologic modeling into a Bayesian network model framework, using the Maumee River Basin as a proof of concept. Our subwatersheds are comparable to the USGS HUC-12 (12-digit Hydrologic Unit Code) watersheds, the national hydrologic unit of the United States ranging in size from approximately 10,000 to 40,000 acres (Jones et al., 2022). Our model framework estimates how much phosphorus is released from different subwatersheds by integrating available waterway phosphorus measurements with simulated flow information from the commonly used Soil and Water Assessment Tool (SWAT) hydrologic model (Arnold et al., 2012). Since the phosphorus release is uncertain, we combine the data and model outputs into a probabilistic framework and apply statistically robust Approximate Bayesian Computation (ABC) (Beaumont et al., 2002; Sunnåker et al., 2013) to estimate the distributions of phosphorus release from subwatersheds.

We use Maumee River Basin in Western Lake Erie as a proof of concept because it is the largest contributor of nutrients to western Lake Erie (Scavia et al., 2014; Bingham et al., 2015). Agricultural nutrient runoff has induced recurring eutrophication and harmful algal blooms in Lake Erie throughout recent decades, threatening the water supply for more than 12 million people in the U.S. and Canada (Michalak et al., 2013). The Maumee River Basin (referred to as Maumee hereafter) is the largest basin (16 460 km^2) draining to Lake Erie, covering parts of Ohio, Michigan, and Indiana. It has seen a proliferation of permitted and unpermitted CAFOs over the last 30 years: only 5% of the current (2019) CAFOs were constructed prior to 1990, with 43%, 35% and 17% built during each of the subsequent three decades (EWG, 2019). Growth in the number of CAFOs can lead to either the increase of livestock population, which generates increasing quantities of liquid and solid manure, or the local increase of livestock density, which can lead to locally increasing manure-to-cropland ratio and risk of overapplication (Key et al., 2011).

2. Prior work motivating our probabilistic framework

Most prior attempts to attribute phosphorus to nonpoint sources adopt deterministic hydrologic models, where the phosphorus release from a watershed is a function of flow dynamics, soil properties, land use, and phosphorus availability (Kast et al., 2019; Easton et al., 2007). Commonly used hydrologic models include SWAT (Arnold et al., 2012; Kast et al., 2019), USGS SPARROW (Schwarz et al., 2006), EPA Storm Water Management Model (SWMM) (Gironás et al., 2010), EPA Hydrologic Simulation Program-Fortran (HSPF) (Bicknell et al., 1993), and Dynamic Watershed Simulation Model (DWSM) (Borah et al., 2002). These models use climatic, physiographic (e.g., elevation, land use, soil), and manure or inorganic fertilizer application data to model the phosphorus transport in surface water using a series of physics-based governing equations (Yang et al., 2016; Liu et al., 2020).

Deterministic hydrologic models calibrate numerous model parameters to fit existing flow and water-quality measurements. Calibrated models can quantify the contribution of a certain source type, such as manure, by setting its input to zero and calculating the changes in the simulated phosphorus load (Kast et al., 2021). While these models are powerful for simulating hydrologic processes at the watershed-scale, their modules for simulating multiple nutrient sources and transport processes are significantly more computationally expensive, involve a large number of parameters, and require input data that is not universally available. As a consequence, they can be cumbersome to deploy at the basin scale, inflexible in integrating new water-quality measurements, and unsuitable for areas with limited data availability.

Instead, existing government assessments often utilize simpler, data-driven approaches. It is valuable to distinguish between output- and input-based approaches, which differ primarily in the data they rely on for source attribution and can lead to substantially different results. Output-based approaches rely on existing water-quality measurements from waterways (e.g., Ohio EPA, 2016). The phosphorus contributions of a region bounded by water-quality-monitor locations can be derived using the corresponding measurements. However, within a given watershed, water-quality monitors with continuous observations tend to be sparse and non-uniformly distributed, leading to large and inconsistently sized attribution regions. Consequently, output-based approaches are inevitably limited in their ability to identify spatial variability in pollution.

Input-based approaches (e.g., ELPC, 2014; EWG, 2021; Stackpoole et al., 2019; Sabo et al., 2021) estimate excess phosphorus using a nutrient mass balance formula that subtracts crop uptake from phosphorus inputs. The phosphorus inputs and uptake by crops are constrained by data on manure production, fertilizer application, land use, and crop yield. Excess phosphorus estimates are generally available at annual intervals and are used as a proxy for a region's phosphorus contribution to the waterways (ELPC, 2014; EWG, 2021; Stackpoole et al., 2019; Sabo et al., 2021). However, input-based estimates of excess phosphorus may significantly differ from the actual phosphorus loss to the waterways because of adsorption and transport. As both the application of inorganic fertilizer or manure and the transport of excess nutrients during phases of high precipitation are seasonal, there can also be significant deviations between the annual mean contributions and peaks within shorter time periods. In addition, input-based approaches implicitly assume that manure is applied to provide nutrients for cropland. As a result, input-based approaches may overlook occurrences like excessive manure application as a way of manure disposal (Long et al., 2018), illegal manure discharge to the waterway, or manure pond spills.

To avoid specific assumptions about the level of fertilizer and manure application, we adopt a probabilistic model framework using ABC to integrate the output- and input-based approaches. Fig. 1 contrasts existing deterministic hydrologic models (A) with our model framework (B). Deterministic hydrologic models represent each process related to the input, output, and transport of phosphorus separately, as highlighted by the gray boxes in Fig. 1A. The description of each

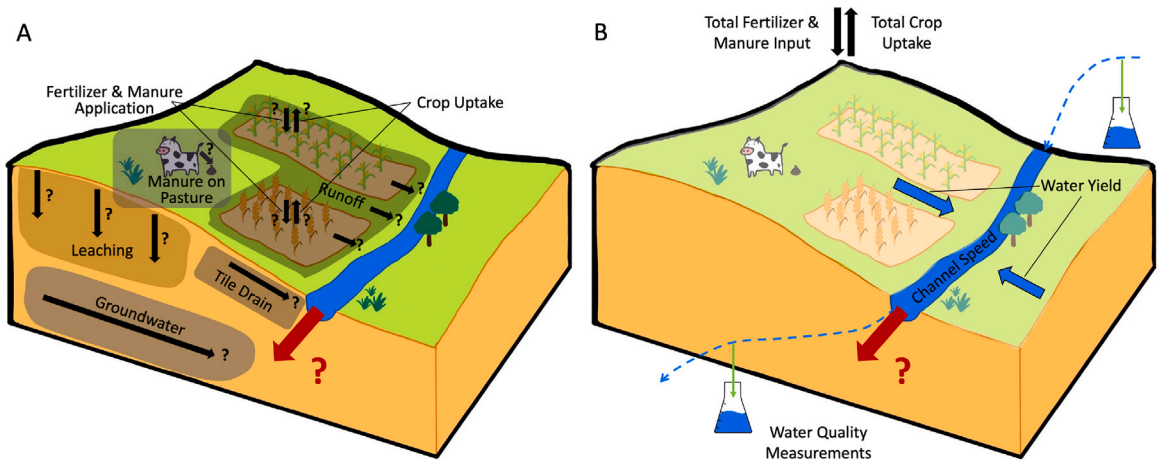

Fig. 1. Comparison between deterministic hydrologic models and our model framework. **(A)**: Illustration of typical processes related to the input, output, and transport of phosphorus. Deterministic hydrologic models simulate the processes to calculate the phosphorus contribution of a subwatershed (red arrow). **(B)**: Illustration of our model framework: namely, quantifying the total phosphorus contributions of subwatersheds using water-quality measurements, the total phosphorus input and output, and the flow information. This framework requires no information on the phosphorus transport processes shown in (A). (For interpretation of the references to color in this figure legend, the reader is referred to the web version of this article.)

process entails multiple parameters that need to be tuned against scarce data, adding significant uncertainty to model projections. Instead of attempting to capture all individual processes despite missing data, our approach attempts to leverage all existing data in a synergistic way by using ABC to combine data on the total phosphorus input and uptake of subwatersheds with water quality measurements and thereby compute subwatershed-scale phosphorus contributions (Fig. 1B). Like other Bayesian approaches, ABC requires the inputs to have probability distributions (priors) from which inputs are sampled to identify distributions of outputs (posteriors) consistent with observations (Beaumont et al., 2002). The priors are constructed following the input-based approaches of excess phosphorus using manure production data, fertilizer application data, crop phosphorus uptake information, and flow information in each subwatershed. We then update the priors with water-quality measurements via ABC to compute the posteriors. We show that the synergy of these data sources enables us to achieve improved spatiotemporal resolutions, accuracy, and efficiency over existing approaches.

3. Methodology

Our model accounts for two forms of phosphorus that can cause eutrophication: the organic or particulate form, called unreactive phosphorus (UP), and the soluble inorganic form, called soluble reactive phosphorus (SRP) (e.g., Søndergaard et al., 2005; Shinohara et al., 2016). Attributing both UP and SRP helps us to estimate the relative contributions of manure and inorganic fertilizer based on their compositional difference. About half of phosphorus in both liquid and solid manure is UP in organic or particulate forms (Fordham and Schwertmann, 1977; Barnett, 1994; Kleinman et al., 2002; Hansen et al., 2004). In contrast, the dominant form of phosphorus in inorganic fertilizer, such as monoammonium and diammonium phosphate (Culman et al., 2020), is phosphate (e.g., Kleinman et al., 2002)—i.e., SRP.

Fig. 2 provides a schematic of our model framework. The main idea behind our model approach, represented by the top box in Fig. 2, is using Approximate Bayesian Computation (ABC) to efficiently evaluate numerous prior samples derived from data-based phosphorus release estimates against existing water quality measurement and thereby obtain an improved, data-compatible posterior of phosphorus release. First, we construct the prior distribution of phosphorus release from each subwatershed (green box in Fig. 2). Second, we compute the flow information, which includes the water yield and channel speed of subwatersheds, using the SWAT model (yellow box). Water quality monitors alone are insufficient to constrain flow, because they provide river discharge data (USGS, 2016) at a spatial scale coarser than our subwatersheds and do not entail channel speed data. We then input the prior distributions and the flow information into the network model, which simulates the phosphorus transport in stream network. We route samples from the prior distributions of sources through the stream network and compare the modeled phosphorus load at water quality monitors with data. With the posteriors of source contributions that are consistent with water quality measurements, we estimate the relative contributions of manure and inorganic fertilizer (orange box in Fig. 2). Table 1 defines key variables and parameters.

3.1. Network model

In discrete mathematics, a network or graph is a structure consisting of a set of points called nodes, where each pair of nodes that share a given relationship is connected by a line, called an edge. These edges can be directed (e.g., river flowing from an upstream to a downstream node) or undirected (e.g., road connecting two cities). These simple building blocks can be used to construct network models representing interconnected systems in the social, natural, and engineering sciences (Khuller and Raghavachari, 1996; Chinowsky et al., 2008; Pokorádi, 2018). We choose to abstractly represent the river network of Maumee as a directed acyclic network model, where water flows along directed edges and connects at junction nodes, but cannot flow back to a point upstream.

Fig. 3 shows Maumee with its five major tributaries identified: the St. Joseph, St. Marys, Auglaize, Blanchard, and Tiffin Rivers. The lower Maumee River near the city of Toledo is its outlet to Lake Erie. More than two-thirds of Maumee are cropland dominated by corn and soybeans with sparsely distributed urban areas, pasture land, and forests. The soil in the region, composed primarily of silt, clay, and fine sand, has poor drainage capacity with high runoff potential (Myers et al., 2000) but widespread tile drainage increases the drainage capacity of much of the cropland. Table 2 summarizes the data used in our model framework for the case of Maumee.

We design the network model such that it represents each subwatershed, which is a nonpoint source, as a single node. To construct the network model, we divide the stream network (USEPA and USGS, 2012) into segments by the locations of confluences or water quality monitors (USGS, 2016; NCWQR, 2022), such that the area of land draining to the outlet of each segment is approximately at the HUC-12 scale (Jones et al., 2022). Text S1 of the supplementary information provides the details of subwatershed division. The corresponding

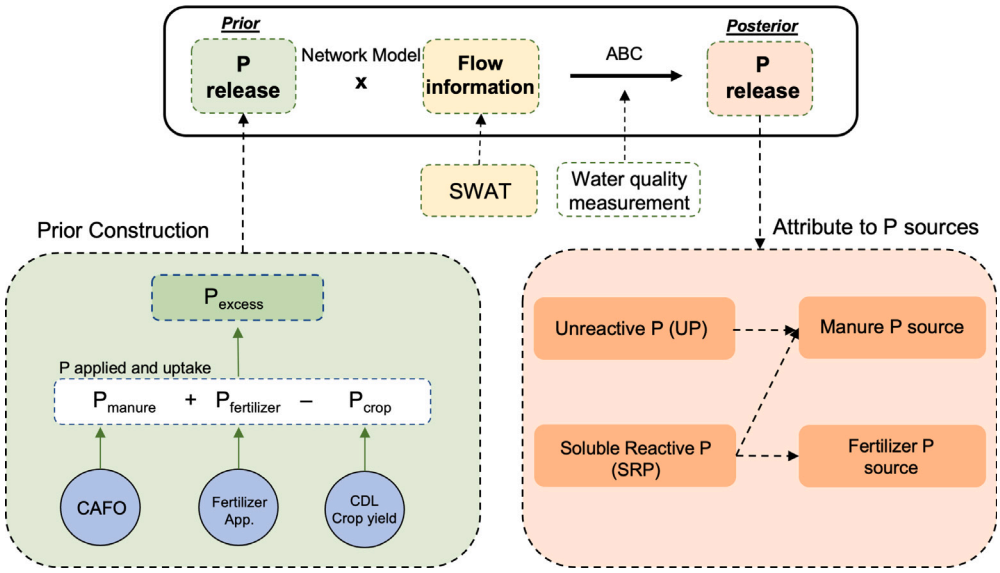

Fig. 2. Model framework. The top box is the model framework comprising the network model, which takes prior distributions (green) and flow information (yellow) as inputs for the forward modeling of nutrient transport, and ABC, which generates posterior distributions (orange). Prior distributions are constructed using data on CAFOs, fertilizer application, and crop type, area, and yield. Based on the posteriors of UP and SRP, we estimate the relative contributions of manure and inorganic fertilizer. (For interpretation of the references to color in this figure legend, the reader is referred to the web version of this article.)

Table 1
Definitions and units of key variables and parameters.

Name	Definition	Unit
Network model		
$D_q()$	Forward modeling function mapping sources S to monitor node q	
D_q^o	Observed nutrient mass at monitor node q	
$W_{s,t}$	Water yield from source node s at time t	m^3
Approximate Bayesian Computation (ABC)		
p_s	Prior distribution of nutrient concentration	
θ	An individual sample: a $\lvert S\rvert \times T$ matrix where each entry $\theta_{s,t}$ contains the mass at source node s at time t	g
t	Time index	days
T	Total simulation time period	days
N	Number of samples drawn in ABC	
n	Number of samples accepted in ABC	
d_q	Relative ℓ_1 distance between modeled and observed mass at monitor q	
w	Length of simulation window	days
Prior distribution		
α	Parameter of beta prime distribution	
β	Parameter of beta prime distribution	
m	Excess nutrient mass	g
C	Set of all CAFOs	
Z	Set of all Counties	
Relative contributions of manure, fertilizer, and legacy phosphorus		
U	Mass of UP contribution of a subwatershed	g
R	Mass of SRP contribution of a subwatershed	g

Table 2
Types and sources of data used in this study for Maumee.

Type	Source	Spatial	Temporal	Reference
Network model setup				
Water quality	NCWQR, USGS	26 stations	Daily	USGS (2016), NCWQR (2022)
River discharge	USGS	58 stations	Daily	USGS (2016)
Stream network	NHDPlusV2	HUC-12	Present	USEPA and USGS (2012)
Inputs to prior formulation				
CAFO	EWG	Point	1988-Present	EWG (2019)
County-level manure rate	USGS	County level	2002–2017	Falcone (2021)
Fertilizer rate	USGS	County level	2002–2017	Falcone (2021)
Land use and crop	USDA-NASS	30-m	2002–2021	Boryan et al. (2011)
Crop yield	USDA-NASS	State level	2006–2021	USDA-NASS (2021)
Climate data				
DAYMET climate	ORNL	1 km	1980-Present	Thornton et al. (2020)

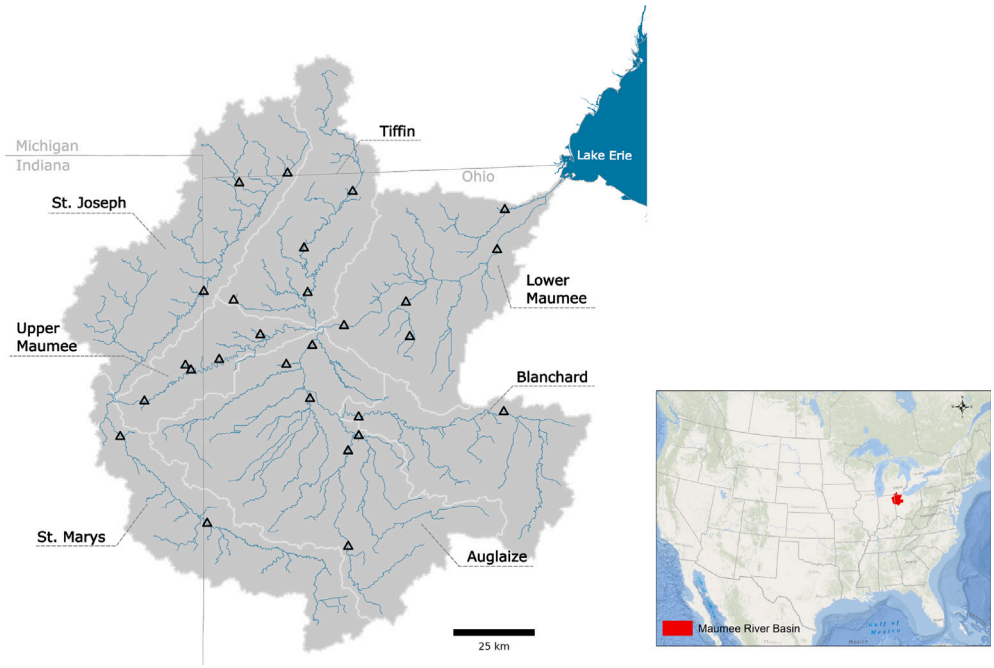

Fig. 3. The Maumee River Basin. Seven HUC-8 watersheds are shown with white boundary lines. The watershed outlet is at Lake Erie on the eastern side. The basin is part of three states: Ohio, Michigan and Indiana. The USGS water-quality measurement locations are shown with black triangles. The inset shows the location of the Maumee River Basin in North America.

drainage area of each segment outlet forms a subwatershed in our model. We place a source node at the outlet of each subwatershed, wherein the nutrient contribution of each source node is attributable to the corresponding subwatershed. Each source node receives an incoming nutrient load and adds its nutrient contribution.

We then insert monitor nodes and junction nodes into the simplified stream network at the locations of water quality monitor stations and river confluences, respectively. The monitor nodes provide locations for comparing simulated nutrient load with water quality measurements without modification. The junction nodes combine incoming nutrient load from upstream branches. Fig. 4A provides an overview of the resultant network. Fig. 4B illustrates the node relationships. The length of the edge connecting each node is defined to be the length of the adjoining channel. Some edges connecting source nodes to monitor or junction nodes have zero length (dashed arrows in Fig. 4B), because we place source nodes at the outlet of subwatersheds, of which the division is based on the locations of confluences or water quality monitors.

We assume that the nutrient contributions of source nodes are non-negative. The water quality measurements support this assumption by showing higher nutrient loads at all monitor stations than their upstream monitor stations, except at the Lower Maumee River, where most algal blooms form at Maumee (EWG, 2022). In 2019, the measured phosphorus load at the outlet of the Lower Maumee River watershed was lower than its incoming phosphorus load, likely because of significant consumption and sedimentation caused by algal blooms. Therefore, to ensure the assumption is valid, our network model excludes the Lower Maumee River watershed represented as the empty shape in Fig. 4A, and the network outlet is the monitor node just upstream of the Lower Maumee River.

The monitor nodes divide the complete network model into components (Fig. 4B). We conduct ABC at the scale of these components. Each component contains all the source nodes in the catchment area bounded by a downstream monitor node and its one or multiple neighboring upstream monitor nodes. The downstream monitor node and the upstream monitor node(s) represent the component outlet and inlet(s), respectively. Upstream-most components, such as the top left one in Fig. 4B, have no inlet monitor node.

To compare the nutrient contributions of source nodes against daily observations of nutrient mass (USGS, 2016; NCWQR, 2022), we route nutrients through the sub-network to the downstream monitor node within each component c via advection. To achieve this daily comparison, we model nutrient routing at an hourly time scale, because the nutrient contributions of a source node on a given day may affect the simulated nutrient load at a downstream monitor node for multiple days. Fig. 5 illustrates the nutrient transport in the network model and simulated nutrient load at the monitor nodes with a synthetic example, where a component contains two source nodes and one monitor node at the component outlet.

Figs. 5A and B show the nutrient contributions of sources 1 and 2 from day 1. Fig. 5C shows the node relationships. Nutrients take less than a day to travel from source 1 to the monitor node and more than a day from source 2. Fig. 5D compares the simulated nutrient load at the monitor load with the daily measurements. The nutrient contributions of both sources from day 1 affect the simulated nutrient load for two days. With temporally varied channel speed, the source contributions arriving at monitor nodes may also be unevenly spaced (Fig. 5D). For example, because of the decrease in channel speed followed by increase, the nutrients departing hourly from source nodes are first spread out and then lumped together, creating the low-load hours and peaks, respectively (Fig. 5D).

Using the edge lengths l (m) and hourly channel speed time series $v(t)$ (m/s) along each edge, we compute the time l/v for nutrients departing each upstream node at a given hour to arrive at the downstream node. We assume that nutrients move at the same speed as the water in the channel. With these travel times, we construct the forward-modeling function $D_q()$, which maps the input nutrient mass departing each source node $s \in S_c$ and each upstream monitor node to compute the total mass arriving at the downstream monitor node q over each time step $t \in T$. We then compute the observed mass at q by multiplying the observed daily concentration (g/m^3) and daily discharge (m^3/s) and scaling by 24×3600 to obtain the total daily observed nutrient mass.

3.2. Approximate Bayesian computation

Approximate Bayesian Computation (ABC) is a rejection-based computational method for calculating posterior distributions of unknown

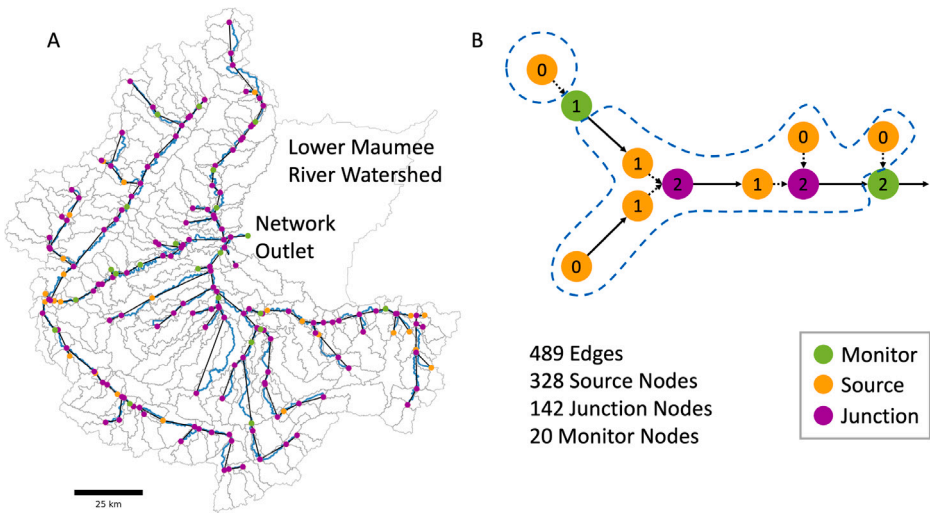

Fig. 4. Network model representation of the stream network at Maumee, with monitor, source, and junction nodes shown with green, yellow and purple points respectively, and edges shown with black arrows. **(A)**: Overview of the entire network model, subwatersheds, and major channels (blue lines). For readability, the source nodes overlapping with junction and monitor nodes are not shown. The empty portion on the right depicts the lower Maumee river watershed. **(B)**: Illustration of node relationships present in the network model. Arrows represent edges, with solid lines representing channels, and dashed lines representing a node connection with zero physical length. The number on each node represents the number of its incoming edges. All nodes have 1 outgoing edge, except the basin-outlet monitor node, which has none. Upstream-most source nodes have 0 incoming edges, while all others have 1. All monitor and junction nodes have 1 and ≥2 incoming zero-length edges from upstream source nodes, respectively (hidden in Fig. 4A). Upstream-most monitor nodes only receive nutrient contributions from associated source nodes and have 1 incoming edge, while the others also receive upstream nutrient load and have 2 incoming edges. The regions bounded by the dashed blue lines illustrate the component division based on the location of monitor nodes. (For interpretation of the references to color in this figure legend, the reader is referred to the web version of this article.)

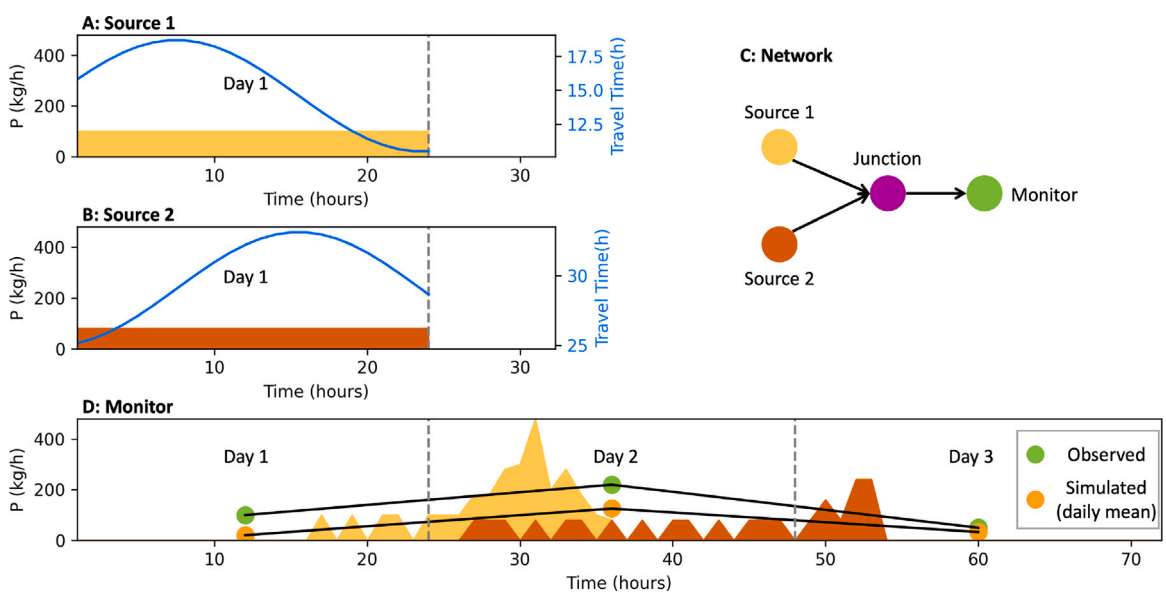

Fig. 5. Illustration of the transport of source contributions and their arrival at a downstream monitor node using a synthetic example. **(A-B)**: Nutrient contributions of sources 1 and 2 in day 1. The blue curves represent the travel time of a phosphorus particle traveling between an upstream source node and a downstream monitor node departing at a certain time. The blue curve represent the travel time under a varied channel speed. **(C)**: Network of the shown example. **(D)**: Nutrient load at the downstream monitor node. The filled curves show the total hourly phosphorus load simulated with the contributions of sources 1 and 2. The green points represent the observed daily phosphorus load. The yellow points represent the daily mean of the simulated phosphorus load. Because the transport time varies over time, the source contributions in adjacent hours may be spread out or lumped together. (For interpretation of the references to color in this figure legend, the reader is referred to the web version of this article.)

model parameters (Beaumont et al., 2002; Csilléry et al., 2010; Sunnåker et al., 2013). In our implementation of ABC, samples of source nutrient contributions are accepted or rejected based on the difference between simulated and observed nutrient loads. Unlike fully Bayesian methods which rely upon complex likelihood functions, ABC is mathematically simple because it bypasses the evaluation of likelihood functions (Sunnåker et al., 2013). While ABC requires evaluating a large number of samples given the large number of sources, this does not pose a problem for our study because the forward modeling of samples through the network is computationally efficient.

We perform ABC independently for each nutrient, so we describe the process for a single nutrient. For each source node $s \in S$, we define a distinct prior distribution p_s over the nutrient concentration. The derivation for p_s is described in detail in Section 3.4. We generate an input mass sample at source s and daily time step t by sampling a concentration from p_s, and multiplying by the daily water yield $W_{s,t}$. The water yield is an output from the SWAT model and is representative of the total outflow from a subwatershed.

In a given component (Fig. 4B), an independent ABC sample $\theta \in \mathbb{R}^{|S_c| \times T}$, is a matrix where a given entry $\theta_{s,t}$ is the mass sampled for a

particular source s and day t, and T is the number of daily time steps in the simulation. We generate N samples from the prior distribution of each source and apply the forward modeling process D_q, generating N sets of outputs for the downstream monitor q. Each output of size $\mathbb{R}^T$ represents the time series of the simulated nutrient load at a given monitor. For each component at the downstream monitor node q, we compare the sample output, $D_q(\theta) \in \mathbb{R}^T$ (yellow points in Fig. 5D), and observations, $D_q^o \in \mathbb{R}^T$ (green points in Fig. 5D), by computing the relative ℓ_1 distance d_q:

$$d_q = \sum_{t=1}^{T} \frac{|D_{q,t}(\theta) - D_{q,t}^o|}{P_{99}(D_q^o)}, \tag{1}$$

where $P_{99}(D_q^o)$ denotes the 99th percentile of the observed daily time series. We normalize the distances by the 99th percentile to both weight each monitor node equally and to trim outliers. We note that when an observed value $D_{q,t}^o$ is missing, the given term is ignored in the summation. For each monitor node q, we accept the n samples resulting in the smallest distance d_q. The accepted samples generate the posterior distribution of the nutrient input of each source node in the component at each daily time step.

To increase computational efficiency and decrease the size of each ABC sample θ, we divide the full simulation period of 365 days in 2019 into smaller windows. We fix a target simulation window of w time steps over the observed monitors and determine the source days such that nutrients departing these sources would arrive at a downstream monitor within the observed simulation window. Thus, we run T/w independent simulations and retain accepted samples only for the corresponding source days of each simulation. Note that this means that each source day posterior is comprised of accepted samples from multiple simulation windows. In this study, we choose $N = 5 \times 10^5$, $n = 50$, and $w = 1$. Higher values of N increase the computation time without significantly increasing the accuracy of the posteriors.

3.3. Hydrologic model

The network model requires subwatershed-scale flow information, including water yield and channel speed, as inputs to calculate nutrient load. Here we use the Soil and Water Assessment Tool (SWAT), a physically based, semi-distributed hydrologic modeling software (Arnold et al., 1998) to simulate the flow information. The SWAT model uses climate forcing data and physiographic data (e.g., soil and land use) to solve for the mass and depth-averaged momentum conservation of water and estimate surface and subsurface flow. Note that our model framework only requires running SWAT once, where we calibrate and validate the model for the years 2015–2020 at Maumee and simulate the flow information. We then use the pre-computed, subwatershed-level water yield and channel speed as inputs to the network model. Details about the SWAT model are included in the supplementary information.

3.4. Prior construction

We assign to each source node s a data-driven prior distribution of nutrient concentration. We use the beta prime distribution as the prior distribution p_s of the nutrient concentrations. The probability density function is defined as

$$p_s(x) = \frac{x^{\alpha-1}(1+x)^{-\alpha-\beta_s}}{B(\alpha, \beta_s)}, \tag{2}$$

where $x > 0$ is the nutrient concentration, $B(\alpha, \beta_s) = \int_0^1 t^{\alpha-1}(1-t)^{\beta_s-1}dt$ is the beta function, and α and β_s are the two parameters of the distribution, where α is a chosen hyperparameter and β_s varies by subwatershed.

We center the prior distribution p_s for each nutrient at the estimated excess phosphorus concentration for subwatershed s discussed in detail below. We then solve for the parameter β_s using the expectation of nutrient concentration over the subwatershed prior $\mathbb{E}(x) = \frac{\alpha}{\beta_s - 1}$ (if $\beta_s > 1$), yielding

$$\beta_s = \frac{\alpha \sum_t^T W_s^t}{U_s} + 1 \tag{3}$$

for β_s for UP. This calculation is defined identically for SRP. We fix $\alpha = 0.5$, which we choose to encourage a large mass near 0, while still allowing for a reasonable probability of sampling larger values.

We estimate excess phosphorus for each subwatershed based on phosphorus mass balance over land. The source term in the phosphorus mass balance formula is the phosphorus input from manure and fertilizer application (EWG, 2019; Falcone, 2021), whereas the sink term is the uptake of phosphorus by crops (Boryan et al., 2011; USDA-NASS, 2021). Manure phosphorus is poorly constrained because of factors like uncertain manure production of CAFOs (EWG, 2019), data withholding (Falcone, 2021), and unknown manure application ranges (Long et al., 2018; Kast et al., 2019). Therefore, we examine three different ways of estimating the excess phosphorus using different data sources and estimation method for manure phosphorus to reduce the bias of the priors, resulting in three different prior distributions. By applying different priors, we can also test the stability of our model framework. We note that the goal of estimating the excess phosphorus is to construct informative prior distributions using the major sources phosphorus with a simple method, rather than achieving highly accurate estimation by considering numerous processes related to the sources and transportation of phosphorus within subwatersheds. The resultant prior distributions are likely inaccurate, but will be correctly by the model framework to create posterior distributions.

We first estimate the annual excess phosphorus mass in subwatersheds and then divide it by the annual water yield from the SWAT model to calculate the concentration. We construct priors separately for UP and SRP. We assume that manure contributes to both UP and SRP, inorganic fertilizer contributes to only SRP, and plants consume only SRP. Therefore, we estimate the excess UP of subwatershed s, U_s, based on the manure production (EWG, 2019; Falcone, 2021) and agricultural land use (Boryan et al., 2011), to be

$$U_s = U_s^m, \tag{4}$$

where U_s^m is the total mass of UP from applied manure in subwatershed s. On the other hand, we estimate the excess SRP of subwatershed s, R_s, based on inorganic fertilizer application (Falcone, 2021), manure application (EWG, 2019; Falcone, 2021), and plant uptake (Boryan et al., 2011; USDA-NASS, 2021), as

$$R_s = R_s^m + R_s^f - R_s^k, \tag{5}$$

where total mass of SRP in subwatershed s is input as applied manure, R_s^m, and applied fertilizer, R_s^f, and output as crop uptake, R_s^k.

3.4.1. Manure phosphorus estimation

We estimate the manure UP and SRP using three different approaches. Figures S3A–F show the results of these approaches. The first approach is based on the CAFO data from EWG (2019). We estimate the manure UP and SRP from each CAFO by the product of animal population, manure produced per animal, and manure phosphorus content. We follow EWG (2019, 2021) and set different manure production rates and phosphorus contents for each major CAFO animal type at Maumee: dairy, cattle, swine, and poultry. Then, assuming the manure is evenly applied to cultivated cropland and pasture within a 10-mile buffer around each CAFO, we calculate the manure phosphorus of a subwatershed by aggregating the intersecting proportions of all CAFO buffers with this subwatershed. We calculate the cultivated cropland and pasture area using the 30-m Cropland Data Layer from the United States Department of Agriculture (Boryan et al., 2011). The assumed 10-mile application buffer is within the range reported by previous studies showing that most manure is applied within short distance around CAFOs (Long et al., 2018; Kast et al., 2019). Without

existing analysis to justify different application ranges for different manure types, we utilize a constant radius for all CAFOs for simplicity. Mathematically,

$$P_s^m = \sum_{c \in C} a_{s,c}^m \gamma_P^c, \tag{6}$$

where P denotes either UP or SRP, C is the set of all CAFOs, $a_{s,c}^m$ is the area of subwatershed s where the cultivated cropland and pasture intersect the manure application buffer of a CAFO c, and γ_P^c is the spatial density of UP or SRP for $c \in C$, defined as:

$$\gamma_P^c = \frac{m^c \phi_P^c}{\sum_{s \in S} a_{s,c}^m + a_{e,c}^m}, \tag{7}$$

where m^c is the manure mass from c, ϕ_P^c is the weight percentage of UP or SRP in the manure type of CAFO c, and $a_{e,c}^m$ is the area of cultivated cropland and pasture outside Maumee that intersects the manure application buffer of CAFO c. We calculate ϕ_P^c following EWG (2021), based on the manure composition data by Barnett (1994) and EWG (2019).

The second approach is based on the USGS county-level data of manure production (Falcone, 2021). We estimate the manure SRP and UP of each subwatershed s by

$$P_s^m = \sum_{z \in Z} a_{s,z}^m \gamma_P^z, \tag{8}$$

where $a_{s,z}^m$ is the cultivated area of subwatershed s intersecting the area of a county z, and γ_P^z is the spatial density of manure UP or SRP application in county z defined as

$$\gamma_P^z = \frac{m^z \phi_P^z}{\sum_{s \in S} a_{s,z}^m + a_{e,z}^m}, \tag{9}$$

where m^z is the manure mass from z, ϕ_P^z is the weight percentage of UP or SRP in the manure type of county z, and $a_{e,z}^m$ is the area of cultivated cropland and pasture outside Maumee that intersects the area of z.

The third approach assumes a uniform manure application across the Maumee. Although this approach smooths out the spatial intricacies of the manure data, it may be the only choice when detailed manure production data are unavailable at the scale of individual CAFOs or counties. We calculate the mean manure UP and SRP of Maumee based on the USGS county-level data of manure production (Falcone, 2021). We then estimate the manure SRP and UP of each subwatershed s by

$$P_s^m = a_s^m \gamma_P, \tag{10}$$

where a_s^m is the cultivated area of subwatershed s, and γ_P is the uniform spatial density of manure UP or SRP application. We calculate γ_P by dividing the total mass of manure UP or SRP application derived in the second approach by the total area of cultivated cropland and pasture.

3.4.2. Fertilizer phosphorus estimation

We estimate SRP from inorganic fertilizer for subwatershed s by multiplying the application rate by cultivated cropland area (Boryan et al., 2011), assuming inorganic fertilizer provides only SRP (Kleinman et al., 2002; Culman et al., 2020). We use county-level inorganic fertilizer application rates over the conterminous U.S. provided by USGS (Falcone, 2021). Mathematically similar to the second approach of computing manure phosphorus (Eqs. (8) and (9)), the SRP from inorganic fertilizer in subwatershed s is

$$R_s^f = \sum_{z \in Z} a_{s,z}^f \gamma_R^z, \tag{11}$$

where $a_{s,z}^f$ is the cultivated area of subwatershed s intersecting the area of a county z, and γ_R^z is the spatial density of fertilizer SRP application in county z defined as:

$$\gamma_R^z = \frac{R_z}{a_{e,z}^f + \sum_{s \in S} a_{s,z}^f}, \tag{12}$$

where R_z is the SRP mass from z, and $a_{e,z}^f$ is the area of cultivated cropland outside Maumee that intersects the area of z. Figure S3G shows the spatial density of fertilizer SRP.

3.4.3. Crop uptake estimation

We estimate subwatershed-scale crop SRP uptake based on the yields (USDA-NASS, 2021), areas (Boryan et al., 2011), and phosphorus uptake rates (Watters, 2021) of different crop types. Mathematically, the SRP uptake in subwatershed s is

$$R_s^k = \sum_{i \in I} a_s^i y_s^i k^i, \tag{13}$$

where I is the set of crop types, a_s^i and y_s^i are the area and yield in s of crop type i, respectively, and k^i is the uptake rate of crop type i. The crop types we consider in I are corn, soybeans, wheat, alfalfa, and other hay. Figure S3H shows the spatial density of SRP uptake via crops.

3.5. Relative contributions of manure, fertilizer, and legacy phosphorus

According to the runoff experiments by Kleinman et al. (2002) and Bertol et al. (2010), applying either inorganic fertilizer or manure increases SRP concentrations in runoff. However, UP concentrations in runoff with and without application of inorganic fertilizer are similar. In contrast, UP concentrations in runoff with manure application is higher than the control and fertilizer groups by a factor of 2. Capturing both UP and SRP can thus help in identifying the relative contribution of manure: Here, we assume that no phosphorus from inorganic fertilizer becomes UP and thus only manure application increases UP concentration in runoff (i.e. $U^f = 0$), yielding the following relationship:

$$U = U^m + U^l, \tag{14}$$

where U^m and U^l denote the contributions of UP mass by manure and legacy phosphorus respectively. The contribution of legacy phosphorus is a function of the baseline phosphorus level, which depends on soil type, the long-term application intensity of manure and fertilizer, and the rate of phosphorus removal via crop uptake or runoff (e.g., Pavinato et al., 2020).

To calculate U^m from the UP obtained from the network model, we first estimate UP from soil, U^l. Kleinman et al. (2002) conducted controlled experiments with high-P and low-P soils and found that UP concentration in runoff is sensitive to soil phosphorus level. Previous studies developed export coefficient models for estimating the phosphorus concentration of runoff (e.g., Winter and Duthie, 2000; Torrent and Delgado, 2001; Sharpley et al., 2002; Easton et al., 2007). However, these models focus on the estimation of dissolved phosphorus, when we also need UP that may largely exist as undissolved particles. We currently lack direct measurements for edge-of-field runoff phosphorus to constrain model parameters.

Instead, we use the measured concentrations of UP and SRP in runoff from the experiments of Sharpley (1997) as an estimate of the soil contribution, because the measured Mehlich-3 P of the soil samples used in Sharpley (1997) is similar to the county-level median Mehlich-3 P at Maumee in 2015 (Dayton et al., 2020). For example, the median Mehlich-3 P levels of Auglaize County in Ohio in 2015 and the soils used in Sharpley (1997) are 33 mg/kg and 25 mg/kg, respectively. We acknowledge that our estimation is uncertain because the Mehlich-3 P of samples within counties are highly variable according to Dayton et al. (2020). For each subwatershed s at time step t,

$$U_{s,t}^l = \min(W_{s,t}[U]^l, U_{s,t}), \tag{15}$$

where $[U]^l$ is the mean UP concentration reported in the control experiments of Sharpley (1997), and $U_{s,t}$ is the UP mass estimated by the network model. We then calculate U^m using Eq. (14) and U^l acquired in the first step.

After calculating the UP contribution of manure for each source and time step, $U_{s,t}^m$, we calculate the SRP contributions by soil and manure. We first calculate the SRP contribution of soil, $R_{s,t}^l$, in the same way as UP using Eq. (15) and the mean SRP concentration reported in the

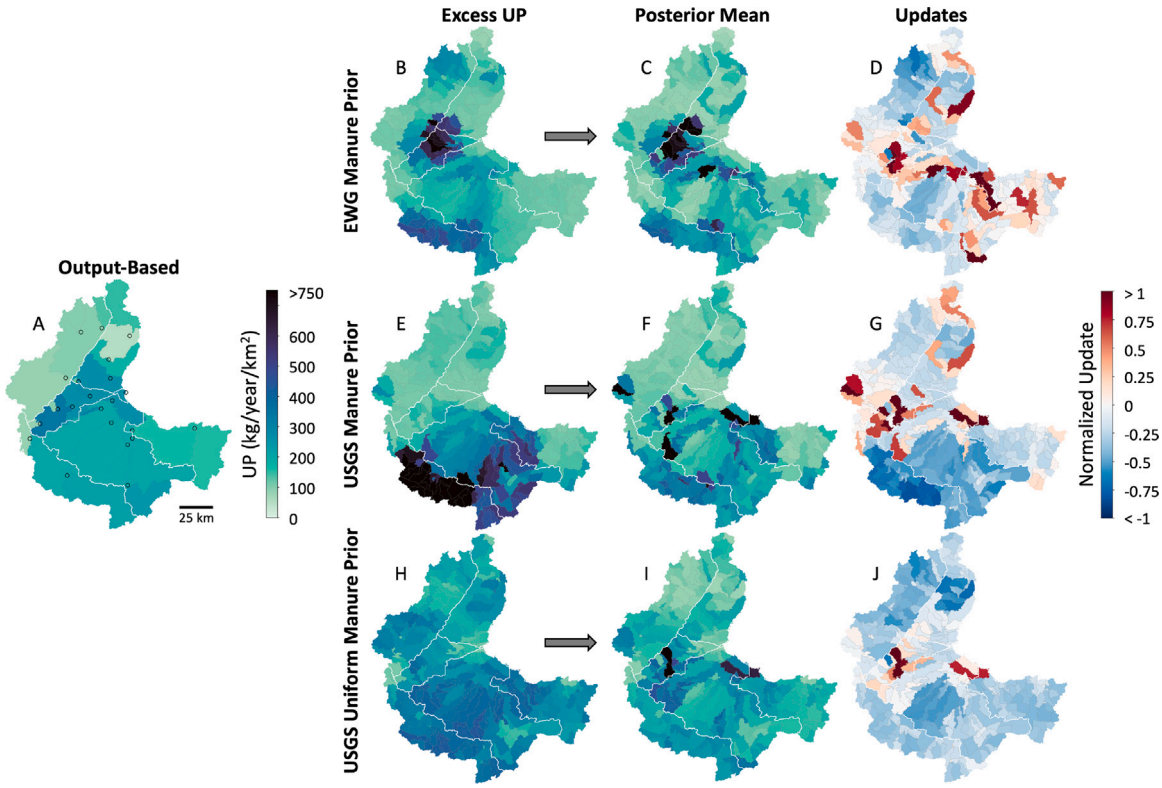

Fig. 6. Spatial distribution of UP. Each row of the second through fourth columns shows one of the three types of prior distributions and the corresponding result. **(A):** Coarse-scale, output-based attribution using only water quality observations with watersheds delimited by monitors (black circles). **(B, E, H):** Fine-scale, input-based attribution using the annual excess phosphorus calculated based on manure, fertilizer, and crop data. **(C, F, I):** Fine-scale attribution using the network model and ABC, which integrates the output-based and input-based approaches. **(D, G, J):** Difference between posterior and prior mean normalized by excess UP, representing updates to priors through the model framework. (For interpretation of the references to color in this figure legend, the reader is referred to the web version of this article.)

control experiments of Sharpley (1997). Then, we calculate the SRP contribution of manure, $R^m_{s,t}$, based on manure compositions. The forms of phosphorus in manure vary with manure forms and animal types. We use the mass ratio $SRP/UP = \lambda = 0.98$ based on the mean value of the data reported in Barnett (1994) to calculate the SRP contribution by manure

$$R^m_{s,t} = \min(\lambda U^m_{s,t}, R_{s,t} - R^l_{s,t}). \tag{16}$$

Therefore, the SRP contribution by inorganic fertilizer is

$$R^f_{s,t} = R_{s,t} - R^m_{s,t} - R^l_{s,t}. \tag{17}$$

4. Results

4.1. Improving spatial inferences in phosphorus release

Recognizing the complementary nature of the input-based and output-based approaches, our model combines both data sources to improve our ability to draw spatial and temporal inferences. We first compare the spatial variability in estimated phosphorus density of our method against the input-based and output-based results with unreactive phosphorus (UP) shown in Fig. 6 and soluble reactive phosphorus (SRP) shown in Fig. 7. The estimates are shown for the year 2019 which we chose to focus on as a proof of concept, because it has more data available than earlier years and is not confounded by the onset of the COVID-19 pandemic.

In the output-based approach (described in Text S4), most of the watersheds are large due to the long distance between monitor nodes (Figs. 6A and 7A). The resulting output-based estimates show nearly homogeneous spatial densities of UP and SRP across the Maumee, with slightly higher UP release density in the watersheds of Upper Maumee, St. Marys and Auglaize, and slightly higher SRP release density in Upper Maumee (for the exact boundaries of these watersheds, see Fig. 3). In contrast, the input-based approach are facilitated by the high spatial resolution of the input land use data (Table 2), resulting in fine-scale subwatersheds comparable in size to USGS HUC-12 scale (Jones et al., 2022) (the second column of Figs. 6 and 7). Our model (the third columns of Figs. 6 and 7) maintains this subwatershed-scale resolution by using highly variable excess phosphorus to construct the prior, but it additionally leverages existing measurements of water quality over time to update the prior. The updates are largest in regions where estimated excess phosphorus does not match the observed nutrient load. The fourth columns (D, G, and J) of Figs. 6 and 7 show the subwatershed-scale updates of the spatial densities of UP and SRP normalized by excess UP and SRP, respectively.

Using different manure data in the input-based approach results in significantly different spatial distribution of excess phosphorus, which is used to construct the priors of our model framework. With the EWG manure prior (EWG, 2019), Fig. 6B shows high excess UP (> 350 kg/year/km^2) availability in St. Marys, Upper Maumee, upper St. Joseph, and pockets of Tiffin and Auglaize—all areas with particularly high CAFO density (see Figure S3 A), which leads to the high UP input from manure in the calculation of excess UP. Fig. 7B suggests that several large regions including southern St. Joseph's and western Blanchard release very little SRP, while very high excess SRP is found throughout Tiffin, along the southwestern border of St. Marys, in upper St. Joseph, and in northern Auglaize. Some of the spatial contrasts coincide with vertical county boundaries at some regions, such as upper St. Joseph and Auglaize, as a result of using the county-level fertilizer application rates (Falcone, 2021).

With the USGS manure prior (Falcone, 2021), where manure data is at the level of counties rather than individual CAFOs, the excess UP (Fig. 6E) and SRP (Fig. 7E) are much higher in St. Marys than in other regions due to the high manure production reported in counties

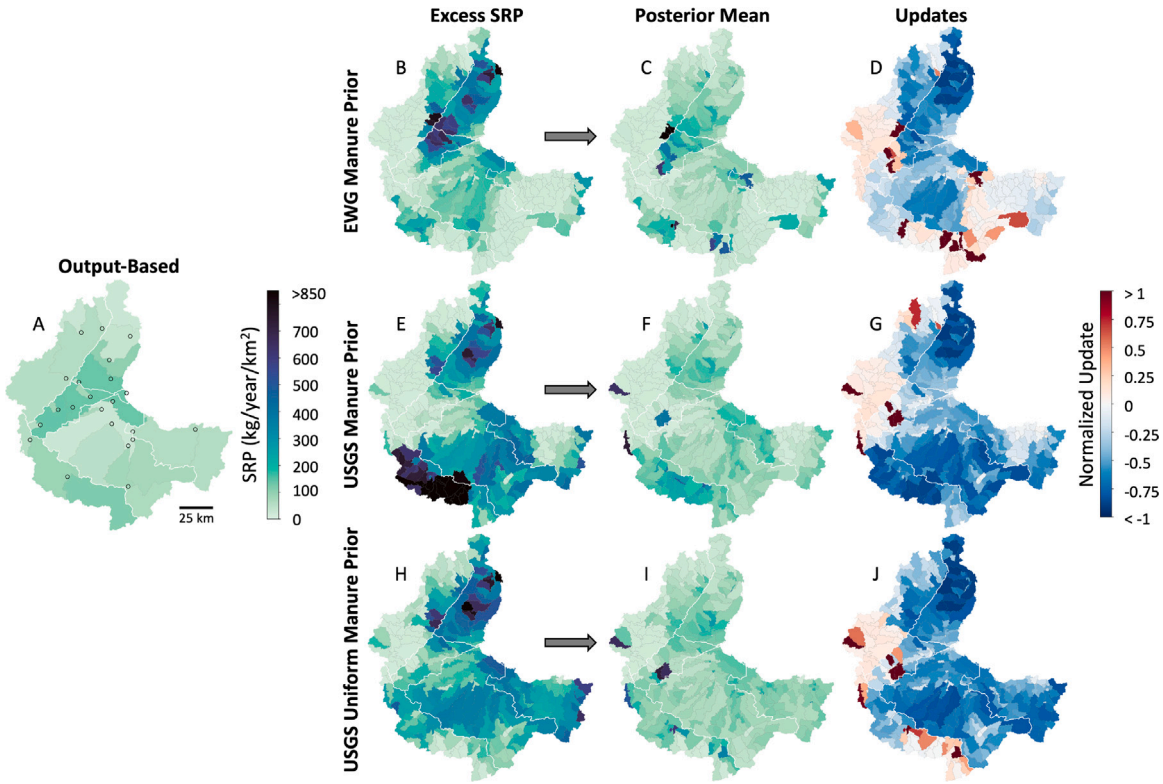

Fig. 7. Spatial distribution of SRP. The captions for sub-figures are the same as Fig. 6.

of St. Marys. The hotspots in Upper Maumee, upper St. Joseph, and Tiffin indicated by the EWG manure prior are not present in the USGS manure prior, likely due to the differences in the spatial resolution and the data collection approaches of the two manure datasets (EWG, 2019; Falcone, 2021). With the uniform manure prior calculated using the USGS county-level manure data averaged across the Maumee, the excess UP (Fig. 6H), which primarily depends on manure data, has lower spatial variability than the other two priors. In contrast, the excess SRP (Fig. 7H), which depends on manure, fertilizer, and crop uptake data, shows hotspots in Tiffin and middle St. Joseph.

The third columns of Figs. 6 and 7 show the fine, subwatershed-scale attribution using our model framework. The results are broadly consistent with the output-based approach (Figs. 6A and 7A) in the sense that subwatersheds of the Upper Maumee, St. Marys, and Auglaize contribute the highest UP levels (Fig. 6C, F, and I), and subwatersheds of the Upper Maumee, St. Marys, and Tiffin contribute the highest SRP levels (Fig. 7C, F, and I). However, our model framework pinpoints the possible regions of peak contribution more specifically than the output-based approach. The model estimates are significantly different from and more consistent with each other than the excess phosphorus in the three priors. For example, the UP hotspot in Upper Maumee indicated in the output-based result and the EWG manure prior but missing in the USGS and uniform manure priors is present in all the posteriors. The model updates significantly reduce the density of UP and SRP release in upper St. Joseph for the EWG manure prior and in St. Marys for the USGS manure prior (the fourth columns of Figs. 6 and 7).

Our model attempts to strike a balance between the output-based and input-based approaches. The spatial heterogeneity suggested by the prior allows the model to disaggregate the often large drainage area between two monitors into subwatersheds with different levels of expected phosphorus release. For example, the two monitor-delimited watersheds constituting St. Marys have estimated UP densities of 209 and 224 kg/year/km^2 in Fig. 6A. Our model considering 72 different subwatersheds within St. Marys estimates UP ranges 62 to 614, 98 to 824, and 83 to 454 kg/yr/km^2 with the three priors, respectively. Meanwhile, our model reduces inconsistencies between estimated nutrient release and measured nutrient concentrations in the streams, leading to a more accurate and spatially smoother attribution than the prior. For example, large excess SRP estimates in the subwatersheds of St. Marys from the USGS manure prior decrease on average by over 50% (Fig. 7G).

The differential updating of expected nutrient contributions flowing to different monitors suggests that our model is able to learn from the available water-quality data. In addition to providing a spatially more nuanced assessment of likely nutrient release, our model resolves one fundamental disconnect between the input-based and output-based models: namely, the input-based model entails significantly higher levels of total nutrient release than the output-based model. Fig. 8 compares the simulated annual UP and SRP mass at monitor stations using excess phosphorus and model posteriors against data. At most monitor stations, using excess phosphorus overestimates the nutrient load, especially for SRP (denoted by triangles). A partial disconnect between excess phosphorus and nutrient transport in streams is not necessarily unexpected, because processes such as manure storage, application approaches, phosphorus storage in the soil, soil erosion, and land-use management alter how much phosphorus is applied and how it is redistributed after application. By integrating the water-quality observations into our model, under all the three largely different priors, the posterior distributions of subwatershed nutrient release are consistent with data (Fig. 8). While the ABC decreases the prior UP and SRP estimates on average, the updates differ at different locations at Maumee (the fourth columns of Figs. 6 and 7), reflecting specific signals from the water-quality measurements.

4.2. Resolving subwatershed-scale daily phosphorus release

Excess phosphorus estimates are generally limited to the annual scale by data availability (e.g., ELPC, 2014). Assuming that the UP or SRP mass from a subwatershed is proportional to its water yield, we can estimate the phosphorus contribution at finer than annual

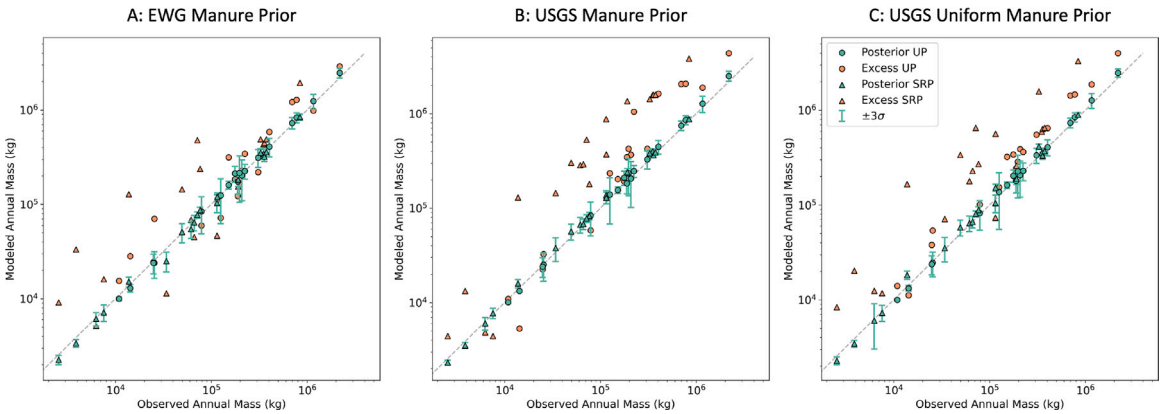

Fig. 8. Simulated annual UP (circles) and SRP (triangles) mass at monitor stations using excess phosphorus (orange) and model posteriors (green) vs. observed annual nutrient mass. The dotted black line represents exact match with data. The error bars represent 3 standard deviations of the simulated mass using the posterior distributions. (For interpretation of the references to color in this figure legend, the reader is referred to the web version of this article.)

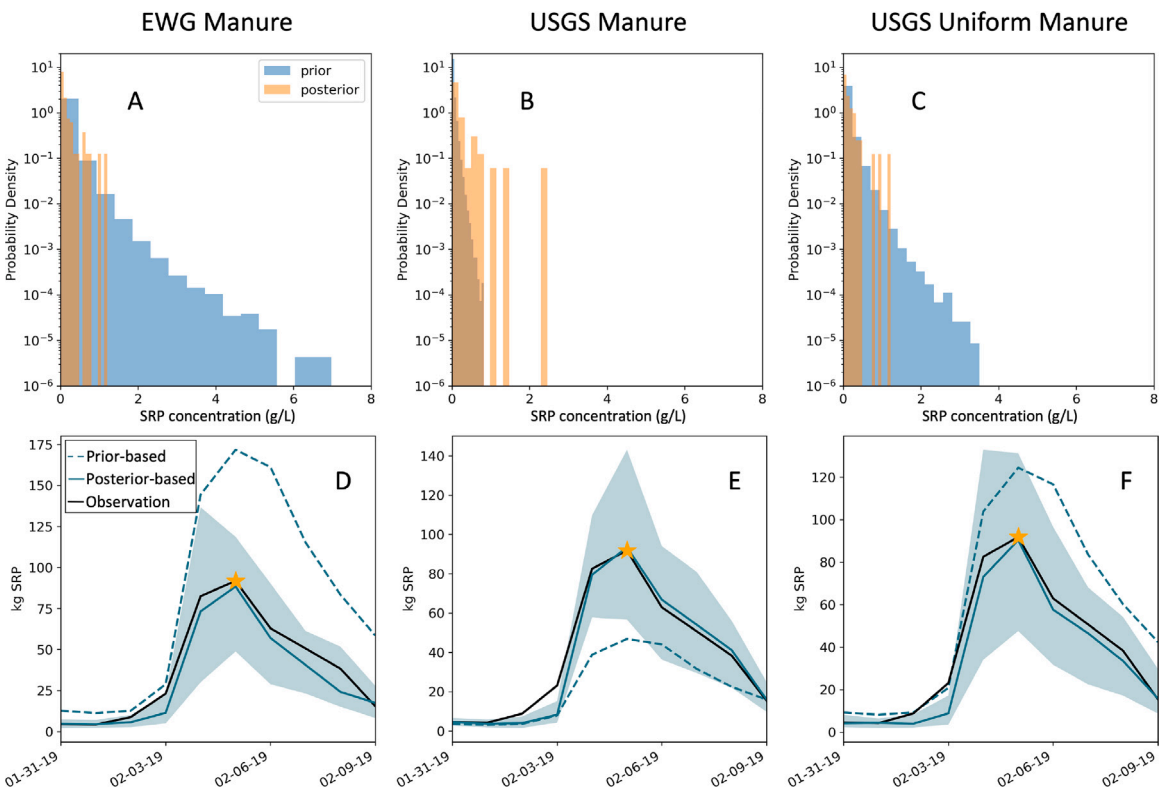

Fig. 9. Example comparison between the prior and posterior distributions. **(A–C):** Prior and posterior SRP distributions of a subwatershed in upper St. Joseph on February 5th, 2019. **(D–F):** Time series of observed SRP mass (solid black curve), prior-based SRP mass simulation using excess SRP (dashed blue curve), and the median with 90% credible interval of simulated SRP mass with posterior SRP distributions (solid blue curve with blue shade) at the downstream monitor node. The yellow star marks February 5th, 2019, the date corresponding to the distributions of A–C. (For interpretation of the references to color in this figure legend, the reader is referred to the web version of this article.)

scales. However, from a practical point of view, it is unrealistic to assume the nutrient concentration remains constant throughout the year, particularly in agricultural areas where seasonal farming patterns influence nutrient release. Incorporating the water-quality measurement time series not only ensures that our model estimates are more consistent with the measurements, but also allows for fine-grained temporal attribution.

Fig. 9 compares the prior and posterior distributions of a subwatershed in upper St. Joseph on February 5th, 2019 as an example of the updating process in our model framework. Figs. 9A–C show the posterior SRP distributions (orange) under the three examined priors (blue). Figs. 9D–F compare the partial time series of simulated SRP mass around February 5th, 2019 at a downstream monitor node based on the different priors and posteriors against the water-quality data. We obtain the prior-based and posterior-based estimates of SRP load in Figs. 9D–F by routing the excess SRP (dashed blue curves) and the 10%, 50%, and 90% quantiles of the posterior (solid blue curves with blue shade) through out network model.

In Figs. 9A and C the posteriors only accept small prior samples and generate distributions mostly constrained below 1 g/L. This update is a consequence of our model rewarding consistency with data as highlighted by Figs. 9D and F where the posterior-based SRP load (solid blue curves) match data (black curves) much more closely than the prior-based SRP load (dashed light blue curves). This analysis suggests that both the EWG manure and USGS uniform manure priors overestimate the SRP release significantly in this subwatershed. In contrast,

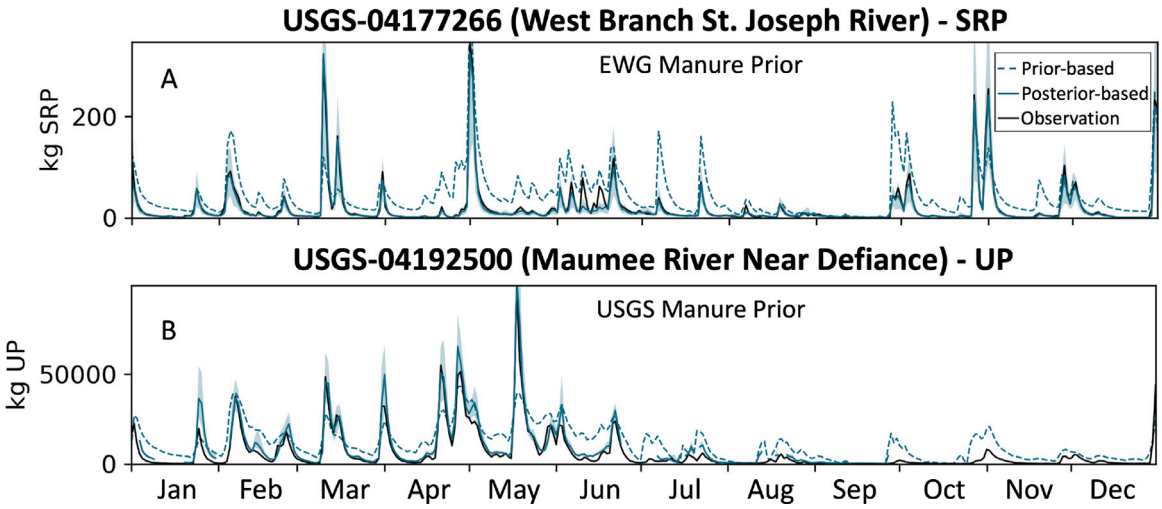

Fig. 10. Comparison between the time series of prior-based, posterior-based, and observed nutrient loads. **(A):** Time series of SRP mass at a relatively low-flow, upstream monitor at upper St. Joseph. The results correspond to the EWG manure prior. **(B):** Time series of UP mass at a relatively high-flow, downstream monitor at the outlet of the study area. The results correspond to the USGS manure prior. The median with 90% credible interval of the mass simulated with posterior distributions are depicted with a solid blue curve with blue shade. The mass simulated with excess phosphorus (prior means) are shown with a dashed blue curve. The observed mass at monitor nodes is shown with a solid black curve. (For interpretation of the references to color in this figure legend, the reader is referred to the web version of this article.)

Fig. 9B shows that the USGS manure prior is largely constrained to small values, resulting in the underestimation of the SRP by the prior in Fig. 9E. To match the data, the posterior distribution in Fig. 9B suggests higher probabilities for large samples (Fig. 9A). Despite the drastically different priors, the posterior distributions are similar in all three cases.

Fig. 9 highlights the disconnect between annual-scale estimates of excess phosphorus and daily-scale observations that leads to either a significant over- or underestimation as shown in panels A, C, D and F and panels B and E, respectively. One possibility for resolving this disconnect would be to introduce a correction factor. However, Fig. 10 shows that the disconnect runs deeper than a single correction factor could capture by highlighting the variability of nutrient loads at smaller time scales. In Fig. 10, we compare the daily time series of prior-based (dashed blue curves) and posterior-based (solid blue curves with blue shade) nutrient load against the water-quality data (solid black curve). Figs. 10A and B show the SRP load at upper St. Joseph and the UP load at a higher-flow, downstream monitor near the outlet of the study area, respectively.

For both Figs. 10A and B, the nutrient load predicted by the posteriors captures the pollution peaks in the water-quality data much better than the priors. In Fig. 10A, the priors underestimate the spikes in March and overestimate the spikes in June and September to October. In Fig. 10B, the priors underestimate the spikes from March to May and overestimate the spikes in June and from September to December. Similarly, the recessions after the peak events are slow and insufficient in the prior-based nutrient load (e.g., dashed curve from March to June in Fig. 10B). Such slow recessions are not present in the observations or nutrient load predicted by the posterior. Finally, the prior-based nutrient load at both monitoring nodes tend to overestimate the nutrient load on low-pollution days, during which the river discharge is also low (USGS, 2016). This overestimation is consistent with water-quality data generally showing lower nutrient concentrations at lower-discharge days (USGS, 2016; NCWQR, 2022), because the priors are computed using annual-scale excess phosphorus.

We note that the nutrient load predicted by the posterior for October to December are missing in Figs. 10B because of the missing water-quality data at monitor station USGS-04183038 in Upper Maumee during this time period. This issue is not uncommon with water-quality measurements and we have partly selected this node partly to provide transparency around this issue. In our analysis, we skip this period when estimating the nutrient release of subwatersheds within the components bounded by this monitor station. Another way of addressing this missing-data issue is ignoring the monitor node in the missing-data period and attributing nutrient release in a larger component. However, a larger component contains more subwatersheds, requires more prior samples, and results in more uncertain posterior distributions.

4.3. Fertilizer contributes more SRP than manure, while manure contributes most of UP

In addition to achieving fine spatial and temporal resolutions, identifying specific source types is a necessary component of phosphorus attribution intended for an actionable nutrient management plan. Most phosphorus entering the streams via rainfall or snow melt runoff is from manure and fertilizer widely applied throughout the basin. Part of this phosphorus comes from newly applied manure and inorganic fertilizer on land surface that have not yet been absorbed by soil. The remainder is from the legacy phosphorus, the combination of the native phosphorus in the soil and the accumulated phosphorus from historical applications (e.g., Pavinato et al., 2020). The legacy phosphorus is present in runoff regardless recent applications (Sharpley, 1997; Kleinman et al., 2002) and is continuously replenished (Nair et al., 1995). Here we ignore the contribution from point sources, such as wastewater treatment plants, because their contributions are much less than nonpoint sources and are outside the scope of this study. According to the estimate of Ohio EPA (2020), nonpoint sources contributes 89% of the phosphorus load at Maumee in 2019.

Figs. 11 and 12 show the spatial distribution of relative contributions of manure, fertilizer and legacy phosphorus as fractions of total annual SRP and UP release at Maumee, respectively. Note that the source type attribution is based on the modeled phosphorus entering the streams for 2019, and the estimates for manure and fertilizer shown in Figs. 11A–F and 12A–C represent the contributions from application over 2019. The contribution of legacy phosphorus shown in Figs. 11G and 12C, however, can include phosphorus accumulated from manure, fertilizer and plant residues from past years.

Figs. 11A–C and 12A–C show substantial spatial heterogeneity in the contributions of manure. For both SRP and UP, high contributions of manure are mainly present in Upper Maumee, St. Marys, and Auglaize. Comparison between the contributions of manure under the three priors with Figures S3A–F shows that the spatial pattern of phosphorus contributions attributed to manure is similar to that of manure phosphorus production, indicating a high impact of manure to the total phosphorus

Fig. 11. Spatial attribution of 2019 surface water SRP sourced from **(A–C)** manure, **(D–F)** fertilizer, and **(G)** legacy phosphorus, which comprises the soil phosphorus from fertilizer, manure, and plant residual accumulated over the years. Each circle represents a fraction of the total annual SRP in the surface water in the study area, where the size is proportional to the contribution. The area of all circles sums up to 1.

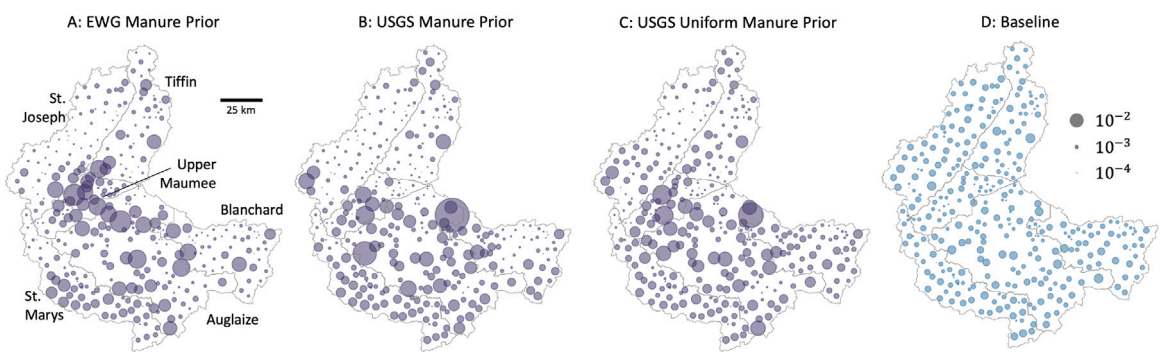

Fig. 12. Spatial attribution of 2019 surface water UP sourced from **(A–C)** manure and **(D)** legacy phosphorus. Each circle represents a fraction of the total annual UP in the surface water in the study area, where the size is proportional to the contribution. The area of all circles sums up to 1.

release. However, the relative phosphorus contributions of subwatersheds, which is the attribution result of our model, significantly differ from the relative magnitude of manure phosphorus production, suggesting that the phosphorus contributed by manure depends on not only manure production, but also other factors that may differ in different regions, such as the treatment before application, application method, and runoff intensity. The attribution results based on the three different priors (Figs. 11A–C for SRP and Figs. 12A–C for UP) also differ less than the data of manure phosphorus production (Figures S3A–C for UP and Figures S3D-F for SRP) used to calculate priors.

Figs. 11D–F show that the contribution of fertilizer is also spatially heterogeneous but in a different way from manure. High contributions of fertilizer are mainly present in upper St. Joseph, Tiffin, Upper Maumee, and St. Marys. In St. Marys and Upper Maumee, both manure and fertilizer show high contributions with locally similar spatial patterns (Figs. 11A–F). This pattern is likely a result of fertilizer application along with excessive manure application that results in release of surplus phosphorus from both sources. In contrast, some other regions, such as part of Tiffin and St. Joseph, show high fertilizer but low manure contributions. These regions coincide with the regions with high fertilizer application in Figure S3G, relatively low crop uptake in Figure S3H, and low manure application in Figures S3A–F. This high-fertilizer and low-manure spatial pattern may indicate excessive fertilizer application in regions without significant manure application.

Figs. 11G and 11D show a significant but lower legacy phosphorus contributions compared with manure and fertilizer. It indicates that the legacy phosphorus, which results from long-term accumulation of phosphorus from different sources, is an important contributor to total phosphorus at Maumee. The homogeneity of the inferred legacy phosphorus contributions throughout the Maumee stems from our assumption of constant baseline UP and SRP concentrations based on experimental data (Sharpley, 1997). In regions where the contributions of both manure and fertilizer are low, such as Blanchard, lower St. Joseph, and upper Auglaize, the legacy phosphorus is likely a major contributor. According to Figure S3, these regions have relatively low manure production, and their fertilizer application rate is below the crop uptake rate.

Table 3 enumerates the SRP and UP release mass by source type in 2019. Figure S4 summarizes the SRP and UP contributions shown in Figs. 11 and 12 at the scale of HUC-8 watersheds (Figs. 3 and 11B).

Table 3
Attribution of phosphorus to manure, fertilizer and base phosphorus for the whole study area with different priors. The attribution represents the outputs for the year 2019.

Prior	UP (tons)	SRP (tons)	Manure SRP (%)	Fertilizer SRP (%)	Legacy SRP (%)	Manure UP (%)	Legacy UP (%)
EWG	5249	1953	35	47	18	66	33
USGS	5160	1868	38	42	20	65	34
Uniform	5187	2026	38	43	19	64	35

Overall, both the total densities and relative contributions of different source types are consistent for the three different priors, except for Upper Maumee (Figure S4), which we discuss in detail in Section 5.2. Both fertilizer and manure are major contributors to SRP, with fertilizer contributing more than or similarly to manure (Figure S4 A). Note that our assumption that fertilizer only contributes to SRP may lead to an overestimation of manure contributions to both UP and SRP. Therefore, this finding indicates fertilizer is likely the top contributor to SRP. As expected under our assumption, manure is the major contributor to UP release in most watersheds (Figure S4B).

4.4. Phosphorus release peaks during spring planting period

Phosphorus transport from land to streams is driven by runoff, slope, soil condition, snow accumulation, and crops (Hansen et al., 2000; Vadas et al., 2011; Zhang et al., 2019). Increased runoff accelerates phosphorus transport, and the transport can potentially increase many-fold if soil is loose and crop roots are short (Blanco-Canqui et al., 2004; Aronsson et al., 2016). Soil particles are generally agitated by precipitation events, with intense precipitation making the land particularly vulnerable to erosion (Sharpley et al., 2008). However, soil agitation, and therefore phosphorus transport, is also a function of crop type and growing stage (Gao et al., 2009; Guo et al., 2019). Crops with larger canopy and widespread root distribution have the ability to reduce soil agitation and hold the soil particles, reducing phosphorus movement compared to non-vegetative areas (Reubens et al., 2007; Zuazo and Pleguezuelo, 2009).

Fig. 13 shows the manure and fertilizer release time series at Maumee along with the precipitation, snow melt, and crop planting and growing periods. For concision, here we only show the results from using the EWG manure prior. The results of other priors are similar. We have extracted the precipitation and snow melt data from DAYMET (Thornton et al., 2020) and display the 3-day rolling mean of these time-series. We estimate snow melt by computing the first-order difference in snow water equivalent between consecutive time steps. We highlight the difference between different crop stages by shading the planting and growing periods of important crops in Ohio and Indiana. The spring planting period for corn and soybeans is April 24 to June 10 (USDA Statistical Reporting Service, 1984). The growing periods of corn and soybeans is July to October (USDA Statistical Reporting Service, 1984; Kast, 2018). The winter wheat planting period is October 1 to November 1 (USDA Statistical Reporting Service, 1984).

Figs. 13A and B demonstrate that SRP and UP from manure are highest during the spring planting season. Fertilizer SRP is also high during this period. This finding can be attributed to three factors. First, frequent and high precipitation increases flow and soil agitation that enhances phosphorus mobility. Second, manure and fertilizer application during the spring planting time means that plenty of phosphorus is available for transport. Third, the underdeveloped roots of newly planted crops have limited ability to retain soil, resulting in relatively high mobility of soil particles, especially without cover crops. In contrast, Figs. 13A and B show the contributions are lower during the growing season (July through October). While precipitation events during growing time tend to be similar to those during the planting period, phosphorus availability is lower later in the year because of increased crop uptake and soil retention by developed root systems. Additionally, by this time phosphorus availability near the surface has decreased due to crop uptake and movement to relatively deeper soil layers.

Snow accumulation and melt control phosphorus transport during the winter months (December through March). At Maumee, most precipitation during this period falls as snow that accumulates over the soil, with several rainfall events leading to melt (Fig. 13C). During the winter months, the overall phosphorus release is relatively low, with manure and fertilizer phosphorus applied during antecedent wheat planting and earlier times covered by snow. Several high phosphorus release events coincide with the snow melt events during February to April (Figs. 13A and B). Snow melt events expose covered phosphorus from earlier fertilizer and manure application and convey it into the streams, possibly along with manure that might have been applied illegally over snow during the antecedent winter (Lewis and Makarewicz, 2009).

5. Discussion

5.1. Filling the gap between the output-based and input-based approaches

The differences between our model estimates and the output-based and input-based approaches beg the question of why these estimates differ. Comparing our model to the output-based approach first, one issue is that the monitor-delimited watersheds in Figs. 6A and 7A differ by more than two orders of magnitude in size, spanning areas from 10 km^2 to 1560 km^2. The higher UP and SRP release densities tend to associate with smaller watersheds of Upper Maumee, suggesting that the heterogeneous sizes of the watersheds may bias estimates: there are potentially other small high-density regions within larger low-density regions, but when aggregated over a large area, the contributions of small regions are smoothed out. The highly heterogeneous attribution suggested by the input-based approach supports the previous argument that the output-based approach is smoothing out extreme values. However, as shown in Figs. 8 and 10, many of these excess phosphorus estimates are inconsistent with water-quality measurements and corrected by our model framework.

The excess phosphorus estimated using a nutrient balance approach with high-resolution land use data (Boryan et al., 2011) and detailed data on manure production from CAFOs (EWG, 2019) has enabled public agencies like Environmental Working Group (EWG) and Environmental Law and Policy Center (ELPC) to map excess phosphorus over watersheds and draw public attention to the problem of excessive agricultural phosphorus input (ELPC, 2014; EWG, 2021). However, the fundamental limitation of the nutrient balance approach is the missing processes connecting phosphorus input and loss. Relevant process include factors like the spatiotemporal variations in runoff intensity, specific agricultural practices, and the biogeochemical evolution of phosphorus forms that are beyond the scope of a simple nutrient balance. In addition, assumptions required to convert input data at various spatial resolutions to the subwatershed scale. For example, in the EWG manure prior, the CAFO locations are points, each with an assumed uniform application range of 10-mile radius. This assumption may deviate from the reality of manure application and introduce artificial sharp contrasts of excess phosphorus between neighboring subwatersheds. Similarly, sharply contrasting estimates sometimes correlate with county boundaries that are unlikely to correspond with drastically different farming practices, such as the low-density western

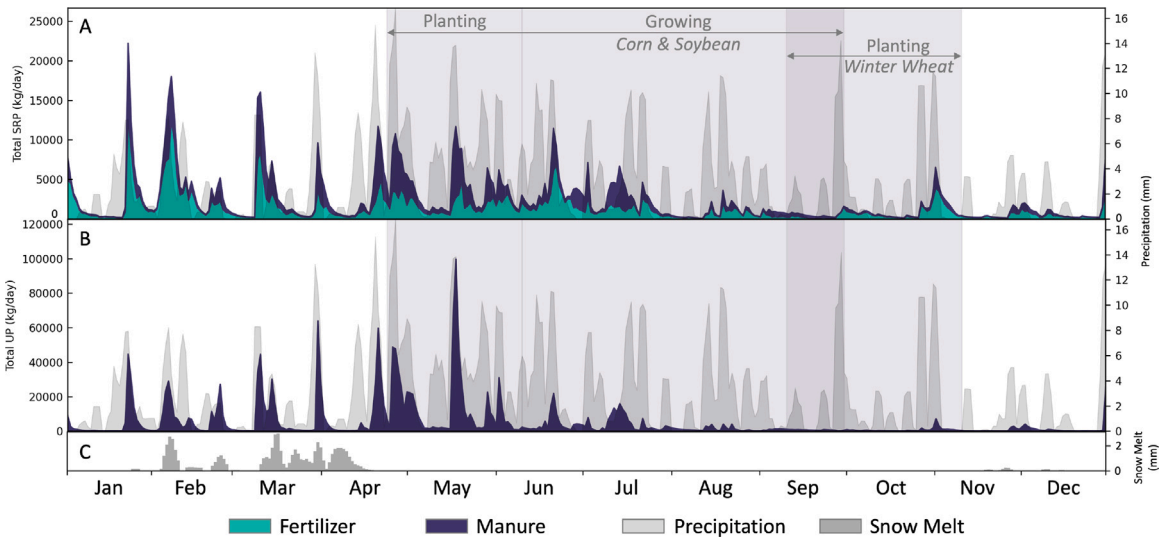

Fig. 13. Daily SRP **(A)** and UP **(B)** mass in the streams at Maumee attributed to manure (purple) and fertilizer (green). Note that in (A) the manure and fertilizer contributions are vertically stacked, with the total curve height showing the total contribution. Precipitation and snow melt time series, smoothed with a 3-days rolling mean, are shown with the light gray shaded area in the top panel and darker gray histogram in the bottom panel. Planting and growing periods for corn and soybeans, as well as the planting period for winter wheat, are depicted with gray shaded rectangles. The contribution from the legacy phosphorus is not shown. (For interpretation of the references to color in this figure legend, the reader is referred to the web version of this article.)

third of the basin and the high-density eastern boundary of Blanchard in Fig. 7B, E, and H.

Our model framework leverages excess phosphorus estimates as a prior, integrates flow information and basic hydrologic routing, and updates the prior by learning from water quality measurements. This updating process removes some of the bias of excess phosphorus in representing phosphorus loss, perhaps most importantly the tendency to overestimate pollution (Fig. 8). Compared with the annual-scale estimates of excess phosphorus, our results also reveal the temporal variation in phosphorus concentration, such as the immense contribution during spring planting and significant loss associated with snow melt (Fig. 13).

As compared to deterministic approaches with computationally expensive hydrologic models (Bicknell et al., 1993; Borah et al., 2002; Schwarz et al., 2006; Gironás et al., 2010; Arnold et al., 2012; Kast et al., 2019), using a more lightweight probabilistic approach like ABC has the advantage of covering numerous possible scenarios and identify the ones that are consistent with data without being biased towards a particular scenario. Although we use a beta prime distribution constructed based on excess phosphorus, the prior distribution for our model framework is flexible based on data availability and specific purposes, making our model framework suitable for application in other watersheds. In the ABC step of this study, we use the simple random sampling scheme, of which the required amount of samples quickly increases with the number of sources. Future work on implementing more advanced sampling schemes can potentially increase the efficiency and scalability of the model framework.

5.2. Ambiguous attribution highlights locations for additional water-quality monitoring

In the three runs for different priors constructed using different manure data (EWG, 2019; Falcone, 2021) and approaches, our model framework generates posterior distributions that are more consistent compared to the largely different priors. For example, the EWG manure prior and the USGS manure prior indicate much higher UP contributions from upper St. Joseph and SRP contribution from lower St. Marys than other priors, respectively (Figs. 6B and 7E). In contrast, the posteriors are similar in these regions (the second columns of Figs. 6 and 7), indicating that the model framework has a stable performance in updating distributions based on water-quality data in these regions.

However, the attribution results in some regions remain ambiguous under different priors. Fig. 14 highlights this issue and exemplifies why these regions require the installation of additional water-quality monitors to achieve high-resolution source attribution. Fig. 14A shows the difference in the UP attribution results between runs with the EWG manure and USGS manure priors to identify subwatersheds with high regional ambiguity. High differences in UP are mainly present in part of Upper Maumee, lower Tiffin, lower St. Joseph, and Auglaize.

The most pronounced region of ambiguity is the component around Defiance, Ohio (the region bounded by bold black line in Fig. 14A), where many subwatersheds show high differences in the results of the two priors. This is a complex component bounded by four upstream monitor nodes. It includes the junctions of Upper Maumee, Tiffin, Auglaize Rivers and other smaller creeks (Fig. 3). Water quality data indicates that this component has overall high spatial densities of UP and SRP release. Attributing nutrients measured in this component is challenging, because they may originate from three major directions as depicted by the yellow arrows in Fig. 14B.

The EWG manure prior suggests high contributions from directions 1 and 2 (Figs. 6B and 7B), while the USGS manure prior implies that most contributions come from direction 3 (Figs. 6E and 7E). Without monitor stations constraining the nutrient load from the three directions, we are unable to achieve confident attributions within this component. The ambiguous attribution results in this component also cause the inconsistent results of source-type attribution for Upper Maumee under the three different priors shown in Figure S4. Depending on the prior, the high nutrient contributions, especially the UP contributions, of this component may be attributed to Upper Maumee, Tiffin, or Auglaize (Fig. 3), with Upper Maumee having the smallest area and thus largest variation in spatial density (Figure S4).

In addition, the phosphorus contribution by the component shown in Fig. 14B also includes non-agricultural point sources from the urban region of Defiance, such as the wastewater treatment plant located near the outlet of the component (empty green circle in Fig. 14B). Point sources only contributes 11% of the phosphorus load at Maumee in 2019 Ohio EPA (2020) and is thus unlikely to affect our source attribution results at a large spatiotemporal scale. However, outside the rainy and snow-melting seasons where the contribution of non-point sources dominate, point sources may bias the source attribution results locally in some subwatersheds. Therefore, it is possible that a

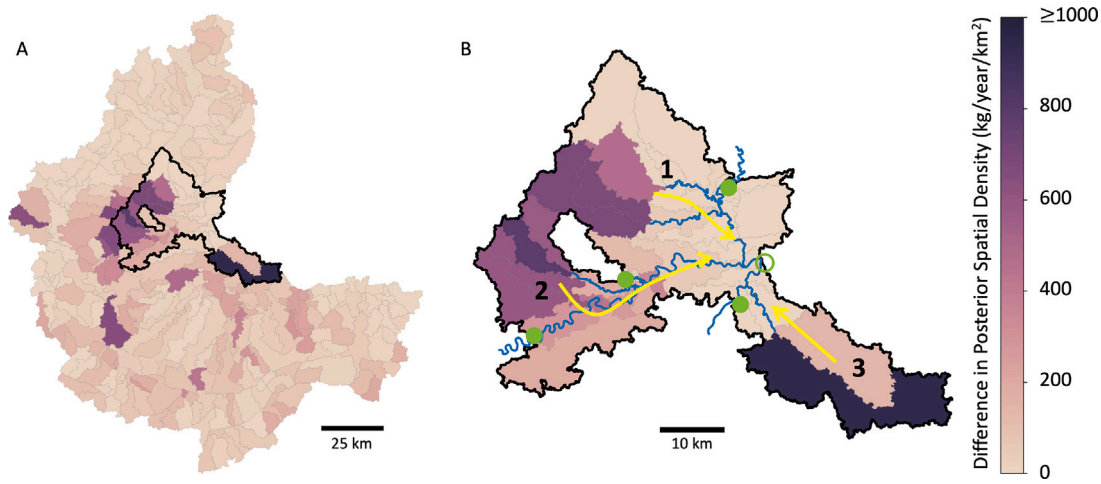

Fig. 14. Difference in the attribution results of UP spatial densities under the EWG manure and USGS manure priors. **(A):** Entire study area. **(B):** Magnified view of the component around Defiance marked by the bold black boundaries in (A). The blue lines are the major streams. The yellow arrows depict the major directions from which the nutrient contributions of the component may originate. The solid green dots mark the upstream monitor stations bounding the component, and the open green circle marks the component outlet. (For interpretation of the references to color in this figure legend, the reader is referred to the web version of this article.)

significant portion of the phosphorus contribution by the component is from the subwatershed near the outlet with the wastewater treatment plant. If additional water-quality monitor stations exist upstream of the wastewater treatment plant, our current model framework can capture its contribution even given a biased prior not considering point sources.

While the presence of these ambiguities indicate that patching together the available data with our model framework is still insufficient in fully achieving high-resolution source attribution in some regions, the ambiguity in attribution can be helpful by identifying locations where the installation of additional water-quality monitor stations would be most impactful. For the marked component in Fig. 14 specifically, it is also valuable to add water-quality monitor stations to the upstream tributaries before the reach the junctions and the wastewater treatment plant. It is also worthwhile for local environmental and agricultural agencies to verify the manure production and application, as the EWG CAFO data (EWG, 2019) and USGS manure data (Falcone, 2021) differ significantly in a region with such high phosphorus contributions.

5.3. Limitations of the model framework

While our model framework improves the spatiotemporal resolution and accuracy of the source attribution of agricultural phosphorus, it is crucial to acknowledge its inherent limitations. We assume that the mass of phosphorus contributed by source nodes are non-negative. Therefore, applying our model framework in streams with significant phosphorus decay caused by sedimentation and algae consumption, such as the Lower Maumee, would require the addition of phosphorus sinks. We also assume that all the phosphorus attributed to subwatersheds are manure, fertilizer, and legacy phosphorus in the soil, while about 11% of the phosphorus load at Maumee are from point sources at 2019 according to Ohio EPA (2020). Although such a relatively low contribution is unlikely to affect our source attribution results at a large spatiotemporal scale, point sources may bias the source attribution results locally near wastewater treatment plants outside the rainy and snow-melting seasons where the contribution of nonpoint sources dominate. Another issue is that our results identify legacy phosphorus as a large contributor to phosphorus concentration (Figs. 11, 12, and S4), but these estimates are highly uncertain, because we assume the baseline concentrations to be constant values taken from runoff experiments (Sharpley, 1997). A more accurate estimation requires incorporating nutrient concentrations of runoff from cropland without recent fertilizer and manure application.

5.4. Applications of the model framework

Additional water-quality data would undoubtedly be incredibly valuable for improving attribution. Because adding new monitors to a stream network is costly, it is useful to evaluate where additional monitors would benefit attribution the most. Our model can help identifying regions with high contributions but ambiguous subwatershed-scale attribution due to the lack of water-quality measurements and disagreements between existing datasets of nutrient input, as illustrated in 5.2. For Maumee, our results show that adding monitors to the complex junction area around Defiance, Ohio, to constrain the contributions from Upper Maumee, Tiffin, Auglaize Rivers and other smaller creeks would be beneficial for reducing ambiguity in source attribution (Fig. 14). As the ambiguous subwatershed-scale attribution is also result of the disagreements between different manure data caused by different data sources and collection method (EWG, 2019; Falcone, 2021), is also beneficial to address these disagreements, which may reveal potential flaws in data collection processes and improve the overall data quality.

While we focus on Maumee in this study, our model framework is generalizable and can be transferred to and customized for the pollution attribution of other areas. It is also lightweight and enables spatial, temporal, and source-specific targeting of the likely most significant contributors without having to purchase and manage large computational resources or conduct labor-intensive monitoring. In this study, generating the attribution results at Maumee for one year only requires hours of computation time on a personal computer or an academic computation cluster. Given the limited resources of public agencies responsible for enforcement, like the U.S. Environmental Protection Agency (EPA), as well as the dearth of high-cadence water-quality monitors, our model framework can augment permitting and enforcement capacity by enabling agencies to focus scarce resources on facilities posing the highest risk. The model inferences can enable evidence-based decisions regarding efficient resource allocation for pollution control. The model framework is also flexible for post-deployment development, such as incorporating new data and method for constructing the priors and adding new water-quality measurements to the network model.

6. Conclusions

This study advances our ability to attribute phosphorus sources by developing a lightweight and generalizable model framework that integrates a nutrient balance derived from data, flow information derived from hydrologic model, and water quality measurements data using Approximate Bayesian Computation. Our model reveals significant spatial,

temporal, and source-type variabilities in phosphorus release, which are averaged out in the coarse-scale attribution by calculating the difference between nutrient load measurements at sparsely deployed monitors. Some subwatersheds of Upper Maumee and St. Marys contribute high quantities of both UP and SRP, with some subwatersheds of Auglaize and Tiffin showing high contributions to each, respectively. The pollution peaks in our results are highly consistent with snow melt and spring rainfall that facilitate runoff. Both inorganic fertilizer and manure are major contributors of phosphorus, with inorganic fertilizer contributing more SRP and manure contributing more UP. Being able to identify such variability can benefit targeted enforcement via prioritizing regions and time periods with higher pollutant release. Our results can also help the prioritization of adding new water quality monitors by demonstrating that the spatial density of monitors is inadequate for achieving confident attributions in some regions with complex tributary junctions, such as the component around Defiance.

CRediT authorship contribution statement

Zihan Wei: Writing – review & editing, Writing – original draft, Visualization, Validation, Software, Methodology, Investigation, Formal analysis, Conceptualization. **Sarfaraz Alam:** Writing – review & editing, Writing – original draft, Visualization, Validation, Software, Methodology, Investigation, Formal analysis, Conceptualization. **Miki Verma:** Writing – review & editing, Writing – original draft, Visualization, Validation, Software, Methodology, Investigation, Formal analysis, Data curation, Conceptualization. **Margaret Hilderbran:** Writing – review & editing, Writing – original draft, Software, Formal analysis. **Yuchen Wu:** Software, Methodology, Investigation, Formal analysis, Conceptualization. **Brandon Anderson:** Writing – review & editing, Software, Resources, Data curation. **Daniel E. Ho:** Writing – review & editing, Supervision, Resources, Project administration, Funding acquisition, Conceptualization. **Jenny Suckale:** Writing – review & editing, Supervision, Resources, Project administration, Funding acquisition, Conceptualization.

Declaration of competing interest

The authors declare the following financial interests/personal relationships which may be considered as potential competing interests: Daniel E. Ho reports financial support was provided by The Chicago Community Trust. Daniel E. Ho reports financial support was provided by Chicago Community Foundation. Daniel E. Ho reports financial support was provided by Stanford Impact Labs. Daniel E. Ho reports was provided by Stanford University Woods Institute for the Environment.

Data availability

The version of our code, v1.1.0, used for the network model framework is preserved at https://doi.org/10.5281/zenodo.8132662 with open access. The usage instructions are provided in the README files of the repository. All the processed data used in the simulation, part of the raw data, and the SWAT simulation results used by the network model framework are preserved at https://doi.org/10.5281/zenodo.8132656 with open access. The code for processing the raw data, which are either in the data repository or publicly available online, is provided in the code repository. The links to the publicly available raw data are also provided in the code repository.

Acknowledgments

This work is supported by Stanford Impact Labs, Stanford Woods Institute for the Environment, The Chicago Community Trust, and Chicago Community Foundation, and by the Stanford Graduate Fellowship in Science and Engineering awarded to ZW. We thank the anonymous reviewers for providing suggestions that greatly improved this article during the revisions.

Appendix A. Supplementary data

Supplementary material related to this article can be found online at https://doi.org/10.1016/j.jenvman.2024.121120.

References

Arnold, J.G., Moriasi, D.N., Gassman, P.W., Abbaspour, K.C., White, M.J., Srinivasan, R., et al., 2012. SWAT: Model use, calibration, and validation. Trans. ASABE 55 (4), 1491–1508.

Arnold, J.G., Srinivasan, R., Muttiah, R.S., Williams, J.R., 1998. Large area hydrologic modeling and assessment part I: Model development 1. J. Am. Water Resour. Assoc. 34 (1), 73–89.

Aronsson, H., Hansen, E., Thomsen, I.K., Liu, J., Øgaard, A., Känkänen, H., Ulén, B., 2016. The ability of cover crops to reduce nitrogen and phosphorus losses from arable land in southern Scandinavia and Finland. J. Soil water Conserv. 71 (1), 41–55.

Baker, L.A., 1992. Introduction to nonpoint source pollution in the United States and prospects for wetland use. Ecol. Eng. 1 (1–2), 1–26.

Barnett, G., 1994. Phosphorus forms in animal manure. Bioresour. Technol. 49 (2), 139–147. http://dx.doi.org/10.1016/0960-8524(94)90077-9, URL https://www.sciencedirect.com/science/article/pii/0960852494900779.

Beaumont, M.A., Zhang, W., Balding, D.J., 2002. Approximate Bayesian Computation in population genetics. Genetics 162 (4), 2025–2035. http://dx.doi.org/10.1093/genetics/162.4.2025.

Bertol, O.J., Rizzi, N.E., Favaretto, N., Lana, M.d.C., 2010. Phosphorus loss by surface runoff in no-till system under mineral and organic fertilization. Scientia Agricola 67 (1), 71–77.

Bicknell, B., Imhoff, J., Kittle, J., Donigian, A., Johanson, R., 1993. Hydrologic Simulation Program—FORTRAN (HSPF) user's manual for release 10. Report No. EPA/600/R-93/174, US EPA Environmental Research Laboratory Athens, GA.

Bingham, M., Sinha, S., Lupi, F., 2015. Economic Benefits of Reducing Harmful Algal Blooms in Lake Erie. Technical Report, Environmental Consulting & Technology, Inc.

Blanco-Canqui, H., Gantzer, C., Anderson, S., Alberts, E., Thompson, A., 2004. Grass barrier and vegetative filter strip effectiveness in reducing runoff, sediment, nitrogen, and phosphorus loss. Soil Sci. Am. J. 68 (5), 1670–1678.

Borah, D.K., Xia, R., Bera, M., et al., 2002. DWSM-a dynamic watershed simulation model. In: Singh, V.P., Frevert, D.K. (Eds.), Mathematical Models of Small Watershed Hydrology and Applications. Water Resources Publications, LLC, Highlands Ranch, Colorado, pp. 113–166.

Boryan, C., Yang, Z., Mueller, R., Craig, M., 2011. Monitoring US agriculture: the US Department of Agriculture, National Agricultural Statistics Service, Cropland Data Layer Program. Geocarto Int. 26 (5), 341–358.

Carleton, J.N., Washington, B.J., 2021. Assessing evidence of phosphorus concentration trends in North American freshwaters. J. Am. Water Resour. Assoc. 57 (6), 956–971. http://dx.doi.org/10.1111/1752-1688.12970, URL https://onlinelibrary.wiley.com/doi/abs/10.1111/1752-1688.12970.

Carpenter, S.R., Caraco, N.F., Correll, D.L., Howarth, R.W., Sharpley, A.N., Smith, V.H., 1998. Nonpoint pollution of surface waters with phosphorus and nitrogen. Ecol. Appl. 8 (3), 559–568.

Chase, J., Benoy, G., Hann, S., Culp, J., 2016. Small differences in riparian vegetation significantly reduce land use impacts on stream flow and water quality in small agricultural watersheds. J. Soil Water Conserv. 71 (3), 194–205. http://dx.doi.org/10.2489/jswc.71.3.194, URL https://www.jswconline.org/content/71/3/194.

Chinowsky, P., Diekmann, J., Galotti, V., 2008. Social network model of construction. J. Construct.Eng. Manag. 134 (10), 804–812.

Csilléry, K., Blum, M.G., Gaggiotti, O.E., François, O., 2010. Approximate Bayesian Computation (ABC) in practice. Trends Ecol. Evol. 25 (7), 410–418. http://dx.doi.org/10.1016/j.tree.2010.04.001, URL https://www.sciencedirect.com/science/article/pii/S0169534710000662.

Culman, S., Fulford, A., Camberato, J., Steinke, K., 2020. Tri-state fertilizer recommendations. Bulletin 974. In: College of Food, Agricultural, and Environmental Sciences. Columbus, OH. The Ohio State University, p. 19.

Dayton, E.A., Shrestha, R.K., Fulford, A.M., Love, K.R., W. Culman, S., Lindsey, L.E., 2020. Soil test phosphorus and phosphorus balance trends: A county-level analysis in Ohio. Agron. J. 112 (3), 1617–1624. http://dx.doi.org/10.1002/agj2.20146, URL https://acsess.onlinelibrary.wiley.com/doi/abs/10.1002/agj2.20146.

Downing, J.A., Polasky, S., Olmstead, S.M., Newbold, S.C., 2021. Protecting local water quality has global benefits. Nat. Commun. 12 (1), 1–6.

Easton, Z.M., Gérard-Marchant, P., Walter, M.T., Petrovic, A.M., Steenhuis, T.S., 2007. Identifying dissolved phosphorus source areas and predicting transport from an urban watershed using distributed hydrologic modeling. Water Resour. Res. 43 (11).

ELPC, 2014. Using Satellite Imagery to Count Animal Feeding Operations. Technical Report, Environmental Law & Policy Center, pp. 1–3, URL https://elpc.org/wp-content/uploads/2020/05/CAFOFactsheet_ELPC_DRAFTv5.pdf.

EWG, 2019. Explosion of Unregulated Factory Farms in Maumee Watershed Fuels Lake Erie's Toxic Blooms. Technical Report, Environmental Working Group, URL https://www.ewg.org/interactive-maps/2019_maumee/.

EWG, 2021. Double Trouble: wisconsin's Land and Water are Inundated with Pollution from Animal Manure and Excess Farm Fertilizer. Technical Report, Environmental Working Group, URL https://www.ewg.org/node/7173/.

EWG, 2022. News Reports of Algae Blooms, 2010 to Present. Environmental Working Group, URL https://www.ewg.org/interactive-maps/algal_blooms/map/.

Falcone, J.A., 2021. Estimates of County-Level Nitrogen and Phosphorus from Fertilizer and Manure from 1950 Through 2017 in the Conterminous United States. Technical Report, US Geological Survey.

Fordham, A.W., Schwertmann, U., 1977. Composition and reactions of liquid Manure (Gülle), with particular reference to phosphate: I. Analytical composition and reaction with poorly crystalline iron oxide (ferrihydrite). J. Environ. Qual. 6 (2), 133–136. http://dx.doi.org/10.2134/jeq1977.00472425000600020006x, URL https://acsess.onlinelibrary.wiley.com/doi/abs/10.2134/jeq1977.00472425000600020006x.

Gao, Y., Zhu, B., Zhou, P., Tang, J.-L., Wang, T., Miao, C.-Y., 2009. Effects of vegetation cover on phosphorus loss from a hillslope cropland of purple soil under simulated rainfall: A case study in China. Nutr. Cycl. Agroecosyst. 85 (3), 263–273.

Gilliam, J.W., 1994. Riparian wetlands and water quality. J. Environ. Qual. 23 (5), 896–900. http://dx.doi.org/10.2134/jeq1994.00472425002300050007x, URL https://acsess.onlinelibrary.wiley.com/doi/abs/10.2134/jeq1994.00472425002300050007x.

Gironás, J., Roesner, L.A., Rossman, L.A., Davis, J., 2010. A new applications manual for the Storm Water Management Model (SWMM). Environ. Model. Softw. 25 (6), 813–814.

Guo, M., Zhang, T., Li, J., Li, Z., Xu, G., Yang, R., 2019. Reducing nitrogen and phosphorus losses from different crop types in the water source area of the Danjiang River, China. Int. J. Environ. Res. Public Health 16 (18), 3442.

Hansen, J.C., Cade-Menun, B.J., Strawn, D.G., 2004. Phosphorus speciation in manure-amended alkaline soils. J. Environ. Qual. 33 (4), 1521–1527. http://dx.doi.org/10.2134/jeq2004.1521, URL https://acsess.onlinelibrary.wiley.com/doi/abs/10.2134/jeq2004.1521.

Hansen, N.C., Gupta, S.C., Moncrief, J.F., 2000. Snowmelt runoff, sediment, and phosphorus losses under three different tillage systems. Soil Tillage Res. 57 (1–2), 93–100.

Higgs, B., Johnston, A., Salter, J., Dawson, C., 2000. Some aspects of achieving sustainable phosphorus use in agriculture. J. Environ. Qual. 29 (1), 80–87.

Howarth, R.W., Anderson, D., Cloern, J.E., Elfring, C., Hopkinson, C.S., Lapointe, B., et al., 2000. Nutrient pollution of coastal rivers, bays, and seas. Issues Ecol. (7), 1–16.

Jones, K., Niknami, L., Buto, S., Decker, D., 2022. Federal standards and procedures for the national Watershed Boundary Dataset (WBD)(5 ed.): U.S. Geological Survey Techniques and Methods 11-A3, 54 p.. Technical Report, U.S. Geological Survey, URL https://doi.org/10.3133/tm11a3.

Jordan, T.E., Whigham, D.F., Hofmockel, K.H., Pittek, M.A., 2003. Nutrient and sediment removal by a restored wetland receiving agricultural runoff. J. Environ. Qual. 32 (4), 1534–1547. http://dx.doi.org/10.2134/jeq2003.1534, URL https://acsess.onlinelibrary.wiley.com/doi/abs/10.2134/jeq2003.1534.

Kast, J.B., 2018. Manure Management in the Maumee River Watershed and Watershed Modeling to Assess Impacts on Lake Erie's Water Quality (Ph.D. thesis). The Ohio State University.

Kast, J.B., Apostel, A.M., Kalcic, M.M., Muenich, R.L., Dagnew, A., Long, C.M., Evenson, G., Martin, J.F., 2021. Source contribution to phosphorus loads from the Maumee River Watershed to Lake Erie. J. Environ. Manag. 279, 111803. http://dx.doi.org/10.1016/j.jenvman.2020.111803, URL https://www.sciencedirect.com/science/article/pii/S030147972031728X.

Kast, J.B., Long, C.M., Muenich, R.L., Martin, J.F., Kalcic, M.M., 2019. Manure management at Ohio confined animal feeding facilities in the Maumee River Watershed. J. Gt. Lakes Res. 45 (6), 1162–1170.

Keiser, D.A., Shapiro, J.S., 2019. US water pollution regulation over the past half century: Burning waters to crystal springs? J. Econ. Perspect. 33 (4), 51–75.

Key, N., McBride, W.D., Ribaudo, M., Sneeringer, S., 2011. Trends and developments in hog manure management: 1998–2009. In: USDA, Economic Research Service, Economic Information Bulletin, no. 81.

Khuller, S., Raghavachari, B., 1996. Graph and network algorithms. ACM Comput. Surv. 28 (1), 43–45.

Kleinman, P.J.A., Sharpley, A.N., Moyer, B.G., Elwinger, G.F., 2002. Effect of mineral and manure phosphorus sources on runoff phosphorus. J. Environ. Qual. 31 (6), 2026–2033. http://dx.doi.org/10.2134/jeq2002.2026, URL https://acsess.onlinelibrary.wiley.com/doi/abs/10.2134/jeq2002.2026.

Kumar, R.R., Park, B.J., Cho, J.Y., 2013. Application and environmental risks of livestock manure. J. Korean Soc. Appl. Biol. Chem. 56 (5), 497–503.

Lewis, T.W., Makarewicz, J.C., 2009. Winter application of manure on an agricultural watershed and its impact on downstream nutrient fluxes. J. Gt. Lakes Res. 35, 43–49. http://dx.doi.org/10.1016/j.jglr.2008.08.003, URL https://www.sciencedirect.com/science/article/pii/S038013300900046X. Special issue on Watershed Management and Nearshore Lake Water Quality, The Conesus Lake Watershed Study.

Liu, Y., Li, H., Cui, G., Cao, Y., 2020. Water quality attribution and simulation of non-point source pollution load flux in the Hulan River basin. Sci. Rep. 10 (1), 1–15.

Long, C.M., Muenich, R.L., Kalcic, M.M., Scavia, D., 2018. Use of manure nutrients from concentrated animal feeding operations. J. Gt. Lakes Res. 44 (2), 245–252. http://dx.doi.org/10.1016/j.jglr.2018.01.006, URL https://www.sciencedirect.com/science/article/pii/S0380133018300078.

Michalak, A.M., Anderson, E.J., Beletsky, D., Boland, S., Bosch, N.S., Bridgeman, T.B., et al., 2013. Record-setting algal bloom in Lake Erie caused by agricultural and meteorological trends consistent with expected future conditions. Proc. Natl. Acad. Sci. 110 (16), 6448–6452.

Myers, D.N., Metzker, K.D., Davis, S., 2000. Status and trends in suspended-sediment discharges, soil erosion, and conservation tillage in the Maumee River Basin–Ohio, Michigan, and Indiana. In: Water-Resources Investigations Report, U.S. Geological Survey, Reston, VA, p. 45. http://dx.doi.org/10.3133/wri004091.

Nair, V.D., Graetz, D.A., Portier, K.M., 1995. Forms of phosphorus in soil profiles from dairies of south Florida. Soil Sci. Am. J. 59 (5), 1244–1249. http://dx.doi.org/10.2136/sssaj1995.03615995005900050006x, URL https://acsess.onlinelibrary.wiley.com/doi/abs/10.2136/sssaj1995.03615995005900050006x.

NCWQR, 2022. National Center for Water Quality Research, sustaining our soil and water resources. URL https://ncwqr.org/.

OC Interagency WQI Workgroup, 2017. Water Quality Indicators (WQI) Project Background and Technical Specifications. Technical Report, US EPA Office of Compliance, URL https://echo.epa.gov/tools/data-downloads/wqi-data-review.

Ohio EPA, 2016. Nutrient Mass Balance Study for Ohio's Major Rivers. Technical Report, Ohio Environmental Protection Agency, Division of Surface Water, Modeling, Assessment and TMDL Section, Columbus, OH.

Ohio EPA, 2020. Nutrient Mass Balance Study for Ohio's Major Rivers 2020. Technical Report, Ohio EPA.

Oliver, S.K., Collins, S.M., Soranno, P.A., Wagner, T., Stanley, E.H., Jones, J.R., Stow, C.A., Lottig, N.R., 2017. Unexpected stasis in a changing world: Lake nutrient and chlorophyll trends since 1990. Global Change Biol. 23 (12), 5455–5467. http://dx.doi.org/10.1111/gcb.13810, URL https://onlinelibrary.wiley.com/doi/abs/10.1111/gcb.13810.

Ongley, E.D., Xiaolan, Z., Tao, Y., 2010. Current status of agricultural and rural non-point source pollution assessment in China. Environ. Pollut. 158 (5), 1159–1168.

Parry, R., 1998. Agricultural phosphorus and water quality: A US Environmental Protection Agency perspective. J. Environ. Qual. 27 (2), 258–261.

Pavinato, P.S., Cherubin, M.R., Soltangheisi, A., Rocha, G.C., Chadwick, D.R., Jones, D.L., 2020. Revealing soil legacy phosphorus to promote sustainable agriculture in Brazil. Sci. Rep. 10 (1), 15615. http://dx.doi.org/10.1038/s41598-020-72302-1.

Pokorádi, L., 2018. Graph model-based analysis of technical systems. IOP Conf. Ser.: Mater. Sci. Eng. 393 (1), 012007.

Reubens, B., Poesen, J., Danjon, F., Geudens, G., Muys, B., 2007. The role of fine and coarse roots in shallow slope stability and soil erosion control with a focus on root system architecture: A review. Trees 21 (4), 385–402.

Sabo, R.D., Clark, C.M., Gibbs, D.A., Metson, G.S., Todd, M.J., LeDuc, S.D., Greiner, D., Fry, M.M., Polinsky, R., Yang, Q., et al., 2021. Phosphorus inventory for the conterminous United States (2002–2012). J. Geophys. Res.: Biogeosci. 126 (4), e2020JG005684.

Scavia, D., Allan, J.D., Arend, K.K., Bartell, S., Beletsky, D., Bosch, N.S., et al., 2014. Assessing and addressing the re-eutrophication of Lake Erie: Central basin hypoxia. J. Gt. Lakes Res. 40 (2), 226–246.

Schwarz, G.E., Hoos, A.B., Alexander, R., Smith, R., 2006. The SPARROW Surface Water-Quality Model: theory, Application and User Documentation. Technical Report, US Geological Survey.

Sharpley, A.N., 1997. Rainfall frequency and nitrogen and phosphorus runoff from soil amended with poultry litter. J. Environ. Qual. 26 (4), 1127–1132. http://dx.doi.org/10.2134/jeq1997.00472425002600040026x, URL https://acsess.onlinelibrary.wiley.com/doi/abs/10.2134/jeq1997.00472425002600040026x.

Sharpley, A.N., Kleinman, P.J., Heathwaite, A.L., Gburek, W.J., Folmar, G.J., Schmidt, J.P., 2008. Phosphorus loss from an agricultural watershed as a function of storm size. J. Environ. Qual. 37 (2), 362–368.

Sharpley, A.N., Kleinman, P.J., McDowell, R.W., Gitau, M., Bryant, R.B., 2002. Modeling phosphorus transport in agricultural watersheds: Processes and possibilities. J. Soil water Conserv. 57 (6), 425–439.

Shen, Z., Liao, Q., Hong, Q., Gong, Y., 2012. An overview of research on agricultural non-point source pollution modelling in China. Separ. Purif. Technol. 84, 104–111.

Shinohara, R., Imai, A., Kohzu, A., Tomioka, N., Furusato, E., Satou, T., Sano, T., Komatsu, K., Miura, S., Shimotori, K., 2016. Dynamics of particulate phosphorus in a shallow Eutrophic lake. Sci. Total Environ. 563–564, 413–423. http://dx.doi.org/10.1016/j.scitotenv.2016.04.134, URL https://www.sciencedirect.com/science/article/pii/S0048969716308270.

Søndergaard, M., Jensen, J.P., Jeppesen, E., 2005. Seasonal response of nutrients to reduced phosphorus loading in 12 Danish lakes. Freshwater Biol. 50 (10), 1605–1615. http://dx.doi.org/10.1111/j.1365-2427.2005.01412.x, URL https://onlinelibrary.wiley.com/doi/abs/10.1111/j.1365-2427.2005.01412.x.

Stackpoole, S.M., Stets, E.G., Sprague, L.A., 2019. Variable impacts of contemporary versus legacy agricultural phosphorus on US river water quality. Proc. Natl. Acad. Sci. 116 (41), 20562–20567.

Stammler, K.L., Taylor, W.D., Mohamed, M.N., 2017. Long-term decline in stream total phosphorus concentrations: A pervasive pattern in all watershed types in Ontario. J. Gt. Lakes Res. 43 (5), 930–937. http://dx.doi.org/10.1016/j.jglr.2017.07.005, URL https://www.sciencedirect.com/science/article/pii/S0380133017301132. Special Section on Lake Ontario CSMI 2013.

Stets, E.G., Sprague, L.A., Oelsner, G.P., Johnson, H.M., Murphy, J.C., Ryberg, K., et al., 2020. Landscape drivers of dynamic change in water quality of US rivers. Environ. Sci. Technol. 54 (7), 4336–4343.

Stoddard, J.L., Van Sickle, J., Herlihy, A.T., Brahney, J., Paulsen, S., Peck, D.V., et al., 2016. Continental-scale increase in lake and stream phosphorus: Are oligotrophic systems disappearing in the United States? Environ. Sci. Technol. 50 (7), 3409–3415.

Sunnåker, M., Busetto, A.G., Numminen, E., Corander, J., Foll, M., Dessimoz, C., 2013. Approximate Bayesian computation. PLoS Comput. Biol. 9 (1), e1002803.

Thornton, M., Shrestha, R., Wei, Y., Thornton, P., Kao, S., Wilson, B., 2020. Daymet: Daily Surface Weather Data on a 1-km Grid for North America, Version 4. ORNL Distributed Active Archive Center, Oak Ridge, Tennessee, USA, http://dx.doi.org/10.3334/ORNLDAAC/1840, URL https://daac.ornl.gov/cgi-bin/dsviewer.pl?ds_id=1840.

Torrent, J., Delgado, A., 2001. Using phosphorus concentration in the soil solution to predict phosphorus desorption to water. J. Environ. Qual. 30 (5), 1829–1835. http://dx.doi.org/10.2134/jeq2001.3051829x, URL https://acsess.onlinelibrary.wiley.com/doi/abs/10.2134/jeq2001.3051829x.

USDA-NASS, 2021. 2021 State Agriculture Overview. Technical Report, United States Department of Agriculture, URL https://www.nass.usda.gov/Statistics_by_State/Ohio/Publications/Annual_Statistical_Bulletin/.

USDA Statistical Reporting Service, 1984. Usual planting and harvesting dates for US field crops, no. 628. US Department of Agriculture.

USEPA, USGS, 2012. NHDPlusV2 (National Hydrography Dataset Plus Version 2). URL https://www.epa.gov/waterdata/nhdplus-national-hydrography-dataset-plus.

USGS, 2016. National Water Information System: USGS Water Data for USA. US Geological Surve, URL https://waterdata.usgs.gov/nwis.

Vadas, P.A., Jokela, W.E., Franklin, D.H., Endale, D.M., 2011. The effect of rain and runoff when assessing timing of manure application and dissolved phosphorus loss in runoff. J. Am. Water Resour. Assoc. 47 (4), 877–886.

Watters, H., 2021. Nutrient Removal for Field Crops in Ohio. Technical Report, Ohio State University, Columbus, Ohio, URL https://ohioline.osu.edu/factsheet/anr-96.

Weil, R., Brady, N., 2017. The Nature and Properties of Soils, fifeenth edition Pearson Education.

Winter, J.G., Duthie, H.C., 2000. Export coefficient modeling to assess phosphorus loading in an urban watershed. J. Am. Water Resour. Assoc. 36 (5), 1053–1061. http://dx.doi.org/10.1111/j.1752-1688.2000.tb05709.x, URL https://onlinelibrary.wiley.com/doi/abs/10.1111/j.1752-1688.2000.tb05709.x.

Yang, X., Liu, Q., Fu, G., He, Y., Luo, X., Zheng, Z., 2016. Spatiotemporal patterns and source attribution of nitrogen load in a river basin with complex pollution sources. Water Res. 94, 187–199.

Zedler, J.B., 2003. Wetlands at your service: Reducing impacts of agriculture at the watershed scale. Front. Ecol. Environ. 1 (2), 65–72. http://dx.doi.org/10.1890/1540-9295(2003)001[0065:WAYSRI]2.0.CO;2.

Zhang, R., Li, M., Yuan, X., Pan, Z., 2019. Influence of rainfall intensity and slope on suspended solids and phosphorus losses in runoff. Environ. Sci. Pollut. Res. 26 (33), 33963–33975.

Zuazo, V.H.D., Pleguezuelo, C.R.R., 2009. Soil-erosion and runoff prevention by plant covers: A review. Sustain. Agric. 785–811.